

A D 7 8 2 8 0

TECHNICAL REPORT

1 July 1970 - 30 June 1971

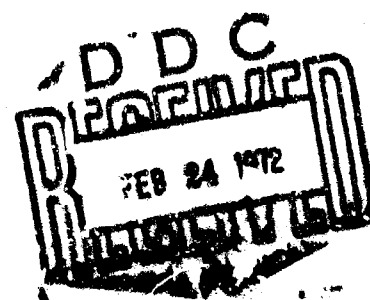
MATERIALS SCIENCES PROGRAM

Reproduced by
NATIONAL TECHNICAL
INFORMATION SERVICE
Springfield, Va. 22151



DISTRIBUTION STATEMENT A	
Approved for public release Distribution Unlimited	

UNIVERSITY OF MARYLAND
CENTER OF MATERIALS RESEARCH
COLLEGE PARK, MARYLAND



ANNUAL TECHNICAL REPORT

SUBMITTED TO THE
ADVANCED RESEARCH PROJECTS AGENCY
OF THE
DEPARTMENT OF DEFENSE

CONTRACT DAHC15-68-C-0211

July 1, 1970 to June 30, 1971

by

CENTER OF MATERIALS RESEARCH
UNIVERSITY OF MARYLAND
COLLEGE PARK, MARYLAND

DISTRIBUTION STATEMENT A

Approved for public release;
Distribution Unlimited

Reproduction in whole or in part is permitted for
any purpose of the United States Government.

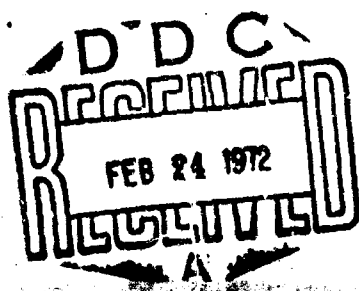


TABLE OF CONTENTS

	<u>Page</u>
I. INTRODUCTION	1
II. RESEARCH PROGRAMS IN MATERIALS SCIENCES	2
A. ELECTRONIC AND MAGNETIC PROPERTIES OF METALS AND ALLOYS	2
1. Electrical Transport Properties of Semi- conducting $Cd_xHg_{1-x}Te$ Alloys (Spain)	2
2. Low-Temperature Resistivity of Bi and Its Alloys (Bhagat)	2
3. Electron Relaxation Rates in Bismuth at Microwave and Far-Infrared Frequencies (Drew)	2
4. Quantum Aspects of the Azbel'-Kaner Resonance in Bismuth (Koch & Drew)	2
5. de Haas-van Alphen Effect in Dilute Alloys of Bismuth in Lead (Anderson)	3
6. dHvA Oscillations in Cobalt Spheres (Anderson)	3
7. Energy Bands in Vanadium at Normal and Reduced Lattice Spacings (Anderson)	3
8. Helicons, Doppler-Shifted Cyclotron Resonance, and Gantmakher-Kaner Oscillations (Falk)	4
9. rf Surface Impedance in the Presence of Mag- netic-Field-Induced Surface States (Koch)	4
10. High-Frequency Damping in a Degenerate Elec- tron Gas (Glick)	4
11. Electroreflectance Observation of Localized and Itinerant Electron States in NiO (Glosser)	5
12. Retardation Effects in Azbel-Kaner Cyclotron Resonance (Drew)	5
13. An Experimental Study of Retardation Effects in Cyclotron Resonance (Koch)	5
14. Magnetic Surface Levels in a Tipped Magnetic Field (Prange)	6

15. An Equation of State of the Noble Metals Based on their Elastic and Cohesive Properties (Bolsaitis) 6
16. Longitudinal Magnetoresistance of Graphite (Spain) 6
17. Ferromagnetic Resonance in Single Crystal Nickel Disks: Angular Dependence of Line-width (Anderson) 6
18. Line Width of Ferromagnetic Resonance in Metals (Prange & Korenman) 7
19. Magnetic Ordering and Low Ni²⁺ Moment in CsNiCl₃ (Minkiewicz) 7
20. Critical and Spin-Wave Fluctuations in Ferromagnets by Neutron Scattering (Minkiewicz) 8
21. Magnetic Critical Phenomena in MnP by Neutron Scattering (Minkiewicz) 8

B. HIGH PRESSURE STUDIES AND EFFECTS

1. The Equation of State of Solid Helium: A Pressure Scale to 20 kbar for High Pressure Measurements at Low Temperature (Spain) 9
2. Pressure Studies of the Fermi Surface of Thallium (Anderson) 9
3. IR Dichroism Study of Polyethylene Crystallized under the Orientation and Pressure Effects of a Pressure Capillary Viscometer (Jackson) 9
4. Direct Microscopic Observation of the Crystallization Process of Polyethylene at High Pressure: Acicular or Bladed Crystals (Jackson & Brasch) 10

C. PHASE TRANSITIONS AND CRITICAL PHENOMENA

1. Neutron Scattering Study of the Lattice Dynamical Phase Transitions in KMnF₃ (Minkiewicz) 11
2. Superconductivity of Beryllium Films (Glover) 11
3. Effect of Surface Charge on the Superconducting Transition Temperature and Normal-State Conductivity of Disordered Metal Films (Glover) 11
4. Depression of T_λ by a Heat Current (Bhagat) 12

5.	The Velocity of Second Sound in a Heat Current (Bhagat)	12
6.	HeII-HeI Transition in a Heat Current: Model Calculations (Bhagat)	12
7.	Photon Counting, Correlation Functions, and the Critical Region (Korenman)	12
8.	Rayleigh Scattering Near the Critical Mixing Point of 3-Methyl-Pentane-Nitroethane (Sengers and Alley)	13
9.	Decoupled-Mode Dynamical Scaling Theory of the Ferromagnetic Phase Transition (Ferrell)	13
10.	Decoupled-Mode Dynamical Scaling Theory of the Binary-Liquid Phase Transitions (Ferrell)	14
11.	Scaling of the Thermal Conductivity Near the Gas-Liquid Critical Point (Sengers)	14
12.	On the Density Expansion for Viscosity in Gases (Sengers)	14
13.	Three-Particle Collisions in a Gas of Hard Spheres (Sengers)	15
D. RADIATION EFFECTS ON MATERIALS		
1.	Berg-Barrett X-ray Observation of Annealing and Laser Induced Damage in Zinc (Lee & Armstrong)	16
2.	A Dynamic Dislocation Pile-up in Neutron-Irradiated Metals (Arsenault)	16
3.	Low Temperature Deformation Characteristics of Neutron Irradiated Vanadium-Titanium Alloys (Arsenault)	16
4.	Melting Behavior of Radiation Crosslinked Crystals of Polyethylene (Jackson)	17
5.	The Application of Radiochromic Dye Film Dosimetry to Medium-Z Absorbers (Silverman)	17
6.	Radiation Induced Polymerization of Pure Styrene at Low Temperature (Silverman)	18
7.	Short-Lived Transient Species in Irradiated n-Hexane (Silverman)	19
8.	Effect of Swelling on Radiation-Induced Grafting of Styrene to Polyethylene (Silverman)	19

9. Dose-Depth Distributions Produced by Electrons
in Multi-Layer Targets (Silverman) 19

E. MECHANICAL PROPERTIES OF MATERIALS

1. Unusual Fracture Features of Oxidized Vanadium +1.31 at .% Titanium Alloy (Arsenault) 21
2. Alloy Strengthening Due to Atomic Order (Marcinkowski) 21
3. Twist Boundaries in Ordered Alloys (Marcinkowski) 21
4. Dislocation Behavior at Grain Boundaries under Heterogeneous Shear (Marcinkowski) 22
5. Thermal Microstresses in Beryllium and other HCP Materials (Armstrong) 22
6. Total Material Variables Influencing a Ductile-Brittle Transition Temperature for Molybdenum (Armstrong) 22
7. Determination of the Frictional Stress for Polycrystalline Iron and Carbon Steels from their Stress-Strain Behavior and its Grain-Size Dependence (Armstrong) 23
8. Fracture of Bone Materials in Compression at Temperatures between -20°C and +200°C (Armstrong) 23
9. Solute-Subgrain Boundary Interaction in Niobium (Armstrong) 23
10. The Critical Resolved Shearing Stress of a Silver 2.9% Indium Alloy as a Function of Growth Rate (Asimow) 24

F. DEVICE TECHNOLOGY

1. Relative Frequency Stability of Stable He-Ne Gas Laser Structures (Hochuli) 25
2. CO₂ Laser Life Study (Hochuli) 25
3. Comparison of Input Offset Voltage of Differential Amplifiers Using Bipolar Transistors and Field-Effect Transistors (Lin) 26
4. Silicon Contract for Area Reduction of Integrated Circuits (Lin) 26

5.	Bi ₂ Se ₃ Hall Effect Magnetometer (Spain)	26
5.	Voltage-frequency Converter uses Four-Layer Diode (O'Haver)	26
7.	The Application of Field-Effect Transistors as Precision Analog Switches in Laboratory Instrumentation (O'Haver)	27

G. SYNTHESIS, STRUCTURE AND REACTIONS OF MATERIALS

1.	Tertiary Phosphine Complexes of Rhodium(III) and Rhodium(I) (Grim)	28
2.	A Phosphorus-31 Magnetic Resonance Study of Tertiary Phosphine Palladium(II) Compounds (Grim)	28
3.	Preparation of 2-diphenylphosphineoethylphosphinites (Grim)	28
4.	Bond Angles, Hybridization and Phosphorus-Metal Bonding (Grim)	28
5.	Upfield and Downfield Shifts in the Nuclear Magnetic Resonance Spectrum of a Tris(Dipivalomethanato) Europium(III) Complex (Mazzocchi & Miller)	29
6.	The Photoisomerization of 2-Cyclopropyl-1-phenylethylene (Mazzocchi)	29
7.	Thermodynamic Equilibria from Plasma Sources. Carbon-Hydrogen-Nitrogen Systems (Lippincott)	29
8.	Reactions of Diboron Tetrahalides with Haloolefins. Formation of Poly(Dihaloboryl)ethanes. (Bellama)	30
9.	Mechanisms for the Thermal Decomposition of Polyethylene (Bailey)	30
10.	A Convenient Preparation of Cyclohexane-1,4-dicarbaldehyde and Cyclohexane-1,1,4,4-tetramethanol (Bailey)	31
11.	New Spiro Polymers Containing Five-, Six-, Seven-, and Eight-Membered Cyclic Ketals (Bailey)	31
12.	A Degradation Study of Some Formaldehyde-Modified Celluloses (B. Smith)	31

13. Cross-Linking of Cotton Cellulose with Ethylene Urea Derivatives Having Varying Hydrogen-Bonding Capabilities. Part I: Effects on the Physical Properties and the Hydrogen-Bonded Structure (B. Smith) 32
14. Crosslinking Cotton Cellulose with Ethylenurea Derivatives Having Varying Hydrogen-Bonding Capabilities. Accessibility Determinations (B. Smith) 32
15. Fusion Behavior of Linear Polyethylene in Dotriaccontane--A DTA Study (T. Smith) 33
16. Acetylene Hydrogenation in a Bubble Column Slurry Reactor (T. Smith) 33
17. Reactions of $\text{Cl}^2\text{P}_{3/2}$: Absolute Rate Constants for Reaction with H_2^3 , CH_4 , C_2H_6 , CH_2Cl_2 , C_2Cl_4 , $\text{c-C}_6\text{H}_{12}$ (Davis) 34
18. A Flash Photolysis - Resonance Fluorescence Kinetics Study of Ground State Sulfur Atoms: I. Absolute Rate Parameters for Reaction of $\text{S}({}^3\text{P})$ with $\text{O}_2({}^3\Sigma)$. (Davis) 35
19. A Flash Photolysis-Resonance Fluorescence Kinetics Study of Ground State Sulfur Atoms: II. Rate Parameters for Reaction of $\text{S}({}^3\text{P})$ with C_2H_4 (Davis) 35
20. Absolute Rate Constants for the Reaction of Atomic Oxygen with 1-Butene over the Temperature Range of 259-493°K (Davis) 36
21. Absolute Rate Constants for the Reaction of Atomic Oxygen with Ethylene over the Temperature Range 232-500°K (Davis) 36
22. Crystal Surface Morphology Developed During The Sublimation of Oriented Zinc Single Crystals (Armstrong & Bolsaitis) 38
23. The Crystal Structure of Methylene Blue (Stewart) 39
24. The Molecular Structure of 1,1-Dimethyl-3-Phenylpyrazolium-5-Oxide (Stewart) 39
25. Scanning Electron Microscope Study of Polyethylene Spherulites (Jackson & Huyinkens) 41
26. Mean-Square Atomic Displacements in HeTe and their Temperature Dependence (Bolsaitis) 42

H. OPTICAL AND SPECTROSCOPIC PROPERTIES OF MATERIALS

- | | | |
|-----|---|----|
| 1. | Optical Absorption of Sodium (Bardasis) | 39 |
| 2. | Single-Crystal Infrared and Raman Spectra
of Cyanuric Chloride (Lippincott) | 39 |
| 3. | Inelastic Neutron Scattering from b.c.c.
^4He (Minkiewicz) | 39 |
| 4. | Vibronic Effects in Hydrogen Bonding
(Lippincott) | 40 |
| 5. | A Linear Technique for the Measurement of
Ultrashort Optical Pulse Widths (Alley) | 40 |
| 6. | Far-Field Diffraction Pattern for Corner
Reflectors with Complex Reflection Coeffic-
ients (Alley) | 41 |
| 7. | GaAs-Laser-Induced Population Inversion in the
Ground-State Hyperfine Levels of CS^{133} (Alley) | 41 |
| 8. | Long Wavelength Phonon Spectra of $\text{Na}_2\text{ZnCl}_4 \cdot 3\text{H}_2\text{O}$
and $\text{Na}_2\text{ZnCl}_4 \cdot 3\text{D}_2\text{O}$ (Lippincott & Khanna) | 42 |
| 9. | Signal-to-Noise Ratio in Atomic Fluorescence
Flame Spectrometry and Condensed-Phase Inor-
ganic Fluorimetry (O'Haver) | 42 |
| 10. | Long Wave-Length Optical Phonons of Sodium
Chlorate at 77°K (Khanna) | 42 |
| 11. | Spectrum and Structure of the He_n Molecule VI.
Characterization of the States Associated with
the UAO's $3p\pi$ and $2s$ (Ginter) | 42 |
| 12. | Electronic Spectra and Structure of the Hydro-
gen Halides. States Associated with the
$(\sigma^2\pi^3)c\pi$ and $(c^2\pi^3)c\sigma$ Configurations of HCl and
DCl. (Ginter) | 43 |
| 13. | Electronic Spectra and Structure of the Hydro-
gen Halides States Associated with the $(\sigma^2\pi^3)c\pi$
$(\sigma^2\pi^3)c\sigma$ Configurations of HBr and DBr
(Ginter) | 43 |

III. FACULTY PARTICIPATING IN MATERIALS RESEARCH PROGRAM	44
IV. RESEARCH ASSOCIATES	45
V. GRADUATE STUDENTS PARTICIPATING IN MATERIALS RESEARCH PROGRAM	48
VI. PUBLICATIONS	50
VII. OTHER SPONSORS	60

SECTION I

INTRODUCTION

This report summarizes the overall program of research in Materials Sciences at the University of Maryland during the period 1 July 1970 through 30 June 1971. Faculty from the Departments of Chemistry, Physics, Molecular Physics, Chemical Engineering and Mechanical Engineering share this effort. Support for this program is derived from several government and military agencies. A specific listing of these sponsors can be found in Section VII. A key portion of the fund is from ARPA (Contract DAHCl5-68-C-0211) and is administered through the Center of Materials Research. These funds are used in direct research support for the purchase of equipment, and for graduate student, research associate, and faculty support. The funds also provide indirect research support through the establishment of a number of central facilities which are available to all materials science research workers.

The research effort is described in detail in Section II. The individual projects have been grouped into eight general areas of research. The faculty member responsible for each project is designated and the sources of funds for a particular project are indicated.

Lists of participating faculty, research associates, and graduate students are provided in subsequent sections. Section VI is a complete listing of the publications which have resulted from the research program.

SECTION II

RESEARCH PROGRAMS IN MATERIALS SCIENCES

A. ELECTRONIC AND MAGNETIC PROPERTIES OF METALS AND ALLOYS

1. Electrical Transport Properties of Semiconducting
 $Cd_xHg_{1-x}Te$ Alloys (Spain)

NASA, ARPA

Measurements of the Hall coefficient have been made as a function of temperature and of magnetic field for semiconducting alloys exhibiting large, negative, low field Hall coefficients at low temperatures. A model is proposed to account for the complex behavior observed in these and in p-type samples.

2. Low-Temperature Resistivity of Bi and Its Alloys (Bhagat)
ARPA, CSIR

The electrical resistivity of pure Bi, Bi-Sb, Bi-Pb, and Bi-Te alloys at $1.3 < T < 77^\circ K$ has been measured. For all the systems the ideal resistivity shows a T^2 -dependence at low temperatures. However, there is a characteristic difference between the compensated (Bi, Bi-Sb) and the uncompensated materials (Bi-Pb, Bi-Te). Several mechanisms, which may account for the data, are discussed.

3. Electron Relaxation Rates in Bismuth at Microwave and Far-Infrared Frequencies (Drew)
AFOSR

Temperature- and frequency-dependent relaxation rates in bismuth have been measured by studies of the magnetic-field-dependent reflectivity of microwave and far-infrared radiation in single-crystal samples. Retardation effects have been taken into account in the analysis of the cyclotron resonance line shapes. The temperature and frequency dependence of the relaxation rates are analyzed in terms of the theory of electron-electron scattering and the experiment provides strong support for electron-electron dominated scattering in bismuth. The experimental results are inconsistent with an electron-phonon dominated scattering mechanism.

4. Quantum Aspects of the Azbel'-Kaner Resonance in Bismuth (Koch & Drew)
Army

Observation is reported of Azbel'-Kaner cyclotron resonance in the limit where distinct transitions between quantized levels have to be considered. A multiplet structure is found in the subharmonic resonances arising from the unequal spacing of the Landau levels in the nonparabolic conduction band of Bi. The data are satisfactorily interpreted in terms of the ellipsoidal-nonparaboloid band-structure model due to lax. The sharpness of the resonances ($\Delta H/H \leq 2\%$) makes it possible to re-examine previously reported band-structure parameters of this model.

5. de Haas-van Alphen Effect in Dilute Alloys of Bismuth in Lead (Anderson)
ARPA

An in situ NMR technique has been used to make accurate (~2 parts in 10^4) measurements of several de Haas-van Alphen frequencies in pure lead for two of the primary symmetry directions, [100] and [110]. By the same method the variation of the [100] β frequency with the addition of up to 0.2% bismuth has been investigated. The alloy results identify the β oscillations as being due to an electronlike piece of Fermi surface. At small impurity concentrations, the dependence of the frequency on concentration is in good agreement with the rigid-band model. However, at the higher concentrations there is a tendency for the frequency changes to be smaller than predicted by the rigid-band model and this trend is interpreted to be due to an increase in the density of states, indicating that electrons are beginning to fill the fourth zone. It is not clear from these results whether the fourth zone begins above or below the pure-lead Fermi energy, but taken at face value, the measurements would suggest that it begins about 4 meV above the Fermi energy.

6. dHvA Oscillations in Cobalt Spheres (Anderson)
AEC

Measurements of the de Haas-van Alphen effect have been made in hcp cobalt spheres in (0001) and (1120) planes. From these measurements information about the Fermi surface and the magnetic field "seen" by the carriers has been obtained.

7. Energy Bands in Vanadium at Normal and Reduced Lattice Spacings (Anderson)
NSF, ARPA

Self-consistent energy band calculations for vanadium were performed by the augmented plane wave method, for different values of the statistical exchange parameter a , at normal and reduced lattice constants. Comparisons have been made with Fermi surface, soft x-ray, photoemission, and elec-

tronic specific heat experiments, and reasonable agreement was found.

8. Helicons, Doppler-Shifted Cyclotron Resonance, and Gantmakher-Kaner Oscillations (Falk)
AFOSR, NRC of Canada

The conductivity of a metal, for the case of the wave vector in the direction of a magnetic field which in turn lies along an axis of p-fold symmetry, is examined. General properties are adduced which explicitly exhibit all the singularities of the conductivity (it is shown that there are no others) and reduce the problem to the conductivity of a collection of cylindrically symmetric Fermi surfaces with progressively smaller weightings. A model, which allows analytic computation, is used for the purpose of examining the possible modes of the electromagnetic field and the Gantmakher-Kaner oscillations. Additional modes, arising from the lack of cylindrical symmetry, are all heavily damped. The Gantmakher-Kaner oscillations are discussed as to damping, amplitude, and position. A general relation between Fermi-surface properties and the optical mass is derived in the absence of phonon effects.

9. rf Surface Impedance in the Presence of Magnetic-Field-Induced Surface States (Koch)
ARPA

The contribution of magnetic surface states to the radio-frequency impedance of metals is considered in the low and high magnetic field limits. A peak in dX/dH is predicted to occur at a field for which the length of a bounce along the skipping trajectory of the first quantum state is comparable to the mean free path. The model is compared with experiments on Cu.

10. High-Frequency Damping in a Degenerate Electron Gas (Glick)
NSF, AFDSR

A closed form has been derived for the dissipative part of the complex frequency- and wave-number-dependent dielectric constant of a degenerate electron gas, $\epsilon(k, \omega)$, valid in the limit $\omega > E_F$, $k < k_F$, where E_F is the Fermi energy and k_F the Fermi wave number. For $\omega > 2E_F$ this expression gives values of $\text{Im}\epsilon(k, \omega)$ which are in excellent agreement with the results of more detailed calculations in which the difficult integrals over phase space were performed by a Monte Carlo method. The formula also appears to give good numerical estimates of $\text{Im}\epsilon(k, \omega)$ for smaller values of ω (but $\omega > k_F/m$), though its accuracy is not assured.

in that region. For example, in aluminum at the plasmon frequency, the asymptotic form agrees with the calculations of DuBois and Kivelson. The high-frequency formula derived may, therefore, be used to circumvent difficult numerical work in estimating the importance of electron correlation effects at high frequencies.

11. Electroreflectance Observation of Localized and Itinerant Electron States in NiO (Glosser)
NSF

Electroreflectance spectra have been observed in NiO at 6eV which is believed to represent transitions from the oxygen 2p derived valence band to the nickel 4s derived conduction band. The spectrum seen earlier by McNatt near 4eV is also observed but interpreted differently in terms of transitions from the localized 3d state to the 4s band. These interpretations are consistent with the recent model of Adler and Feinleib.

12. Retardation Effects in Azbel-Kaner Cyclotron Resonance (Drew)
AFOSR

Corrections to the Azbel-Kaner theory of the magnetic field dependent surface impedance of metals have been calculated. The results illustrate the effects of the finite transit time of the electrons in their passage through the skin layer. The cyclotron resonance line shapes are modified from the Azbel-Kaner results for both the high $\omega \tau$ and low $\omega \tau$ limits. The bearing of these results on experimental determinations of carrier effective masses and relaxation times are discussed. Finally, the background signals from the non-resonant electrons are calculated for an arbitrary cut off angle for specular reflection of the electrons at the surface.

13. An Experimental Study of Retardation Effects in Cyclotron Resonance (Koch)
Army

When the electron transit time through the skin layer becomes comparable to the rf period, Azbel-Kaner cyclotron resonance is substantially altered. As Drew has shown explicitly, the retardation effect leads to an exponentially decreasing amplitude of successive subharmonics and a progressive change of the resonance lineshape. We present and analyze data on a particular non free electron like orbit on the Fermi surface of Ga, which at frequencies in the range 8-54 GHz shows strong retardation. The data confirm the expected exponential decay and related lineshape changes, and give evidence for their frequency and mean free path dependence.

14. Magnetic Surface Levels in a Tipped Magnetic Field
AFOSR, ONR (Prange)

The wave functions and spectrum for metallic electrons skipping along a surface in a magnetic field are calculated for general orientation of field and surface relative to the crystal axes of the material. Unlike the case in which the field is parallel to the surface, the energy levels form a continuum rather than a discrete set of bound magnetic surface levels. Nevertheless, except for rather extreme tip angles, no broadening or change of shape of the observed signals should be observed. In general there will be a rescaling of the field variable which can be used to measure Fermi-surface quantities inaccessible by other techniques. The analysis of the data is somewhat more complex than in the parallel-field case, however.

15. An Equation of State of the Noble Metals Based on their Elastic and Cohesive Properties
AEC (Bolsaitis)

The inclusion of contributions from effects due to Fermi surface distortion in elastic constants of the noble metals as calculated by a Wigner-Seitz cell plus pairwise interionic potential description, results in nearly self consistent Born-Mayer Potential constants. These constants permit the calculation of P-V-T relations in the noble metals, and consequently pressure derivatives and temperature derivatives of the elastic constants in satisfactory agreement with experimental values.

16. Longitudinal Magnetoresistance of Graphite
AEC (Spain)

Measurements of the longitudinal magnetoresistance $\rho_{zz}(H_z)$ of graphite with primary electric current perpendicular to the basal planes ($J \parallel c \parallel H$) are reported in magnetic fields up to 8 tesla (80 kG). Several new features have been observed, including saturation effects at 77°K, the observation of quantum oscillations (Shubnikov de Haas Effect) up to the n=1 Landau level, and further structure in the oscillations at $T = 1.4^{\circ}\text{K}$. The results are compared to the transverse magnetoresistance $\rho_{xx}(H_z)$ and discussed in relation to recently proposed models for c-axis conduction.

17. Ferromagnetic Resonance in Single Crystal Nickel Disks: Angular Dependence of Linewidth
AEC (Anderson)

The angular variation of the FMR linewidth in single crystal disks of nickel has been studied for both the in-plane ($H \parallel$ sample surface) and out-of-plane ($H \perp$ sample surface) geometries. For the in-plane case the linewidth

is essentially isotropic. For the out-of-plane geometry the effective linewidths exhibit a shallow minimum for M about 55° from the sample plane. For both geometries these results are consistent with a Gilbert type equation (including exchange conductivity effects) with an angle independent damping parameter.

18. Line Width of Ferromagnetic Resonance in Metals
ARPA (Prange & Korenman)

Considerable experimental evidence has now been accumulated which indicates that the intrinsic damping of spin waves in metallic ferromagnets can best be described by the Gilbert form of the Landau-Lifshitz equation. The intrinsic decay rate parameter λ can be decomposed into three components, one of which is independent of both temperature and impurity concentration, another which contributes an additional broadening in the immediate neighborhood of the Curie temperature and is doubtless due to effects of critical fluctuations, and a third anomalous contribution, observed experimentally only in quite pure nickel, six times larger than the first contribution at helium temperature, but negligible above about 100°K .

It is proposed that the anomalous contribution is also "anomalous" in the sense of the anomalous skin effect, which prevails when the electron mean free path is long compared with the skin depth. A detailed model is offered in which the magnon can decay directly into an energy and momentum conserving electron-hole pair. These results are compared with the present experimental data, and further tests of the hypothesis is proposed.

19. Magnetic Ordering and Low Ni^{2+} Moment in CsNiCl_3
AEC (Minkiewicz)

The magnetic structure of CsNiCl_3 has been carefully reexamined by single-crystal neutron diffraction techniques in view of an apparent inconsistency between previous powder neutron diffraction results and a recent NMR investigation. Intensity data were collected from two different-sized crystals taken from the sample used in the NMR study, and corrected for absorption and extinction effects. These data confirm that there is an anti-ferromagnetic transition at 4.3°K to the triangular arrangement of moments deduced in the previous study. In the region between 4.3 and 2.7°K the sublattice

magnetization has a critical exponent β of 0.27 ± 0.03 . A particularly striking result is that the magnitude of the Ni^{+2} moment extrapolated to $0^{\circ}K$ is only $(1.0 \pm 0.1)\mu_B$, indicative of very substantial zero-point deviation effects.

20. Critical and Spin-Wave Fluctuations in Ferromagnets by Neutron Scattering

AEC

(Minkiewicz)

The results of neutron scattering experiments on iron and nickel in the critical regime are reviewed and discussed; particular emphasis is placed on the dynamics of the spin fluctuations. Als-Nielsen has demonstrated that, for iron, the perplexing questions concerning the spin diffusion constant and the results of quasi-elastic scattering experiments can be resolved in a natural way by using the scaling function recently calculated by Resibois and Piette. The experimental results for nickel, while not being as complete, are consistent with the relations that are expected among the critical exponents for the spin diffusion constant, the inverse range parameter, and the static susceptibility. The experimental results in the spin-wave and transition regions are in satisfactory accord with theory. The diffusive fluctuations below T_c have never been clearly observed for either iron or nickel. This result is in marked contrast to the experimental results for the antiferromagnets.

21. Magnetic Critical Phenomena in MnP by Neutron Scattering

AEC

(Minkiewicz)

Three-crystal inelastic neutron scattering measurements have been carried out on a single crystal of MnP in the critical region. The compound is ferromagnetic below its ordering temperature of $291.5^{\circ}K$. The results of the experiments have demonstrated that for $T < T_c$, there exists a striking dissimilarity between the profiles observed for MnP on one hand and iron and nickel on the other. We have observed for the first time the diffusive fluctuations in a ferromagnetic for $T < T_c$. These results should be contrasted with those that were previously obtained for iron and nickel. For iron and nickel, these diffusive modes have never been clearly observed. The characteristic frequency of the critical fluctuations $f(\kappa, \zeta)$ for $T = T_c$ is found to be reliably described by the relation $f(0, \zeta) \propto \zeta^x$, where $x = 2.57 \pm 0.11$, and ζ is the reduced wave vector. This result is in excellent agreement with the prediction made from dynamic scaling theory. For the isotropic ferromagnet, the dynamic scaling principle predicts a critical exponent of $5/2$.

B. HIGH PRESSURE STUDIES AND EFFECTS

1. The Equation of State of Solid Helium: A Pressure Scale to 20 kbar for High Pressure Measurements at Low Temperature
AEC, ARPA (Spain)

The use of helium as a pressure transmitting medium enables pressure measurements to be made in a truly hydrostatic environment over the widest possible range of pressures and temperatures. At a low enough temperature, helium freezes. If the freezing process is allowed to occur under constant pressure conditions, shears in the experimental system are reduced to a minimum. A calculation is given in the approximation of the Mie-Gruneisen equation of state of the pressure as a function of temperature along the isochores of helium up to 20 kbar ($1 \text{ kbar} = 10^8 \text{ N m}^{-2}$) enabling a pressure scale to be set up in this range. Numerical estimates of the possible errors made in the calculation are given. Tables are given of the pressure along selected isochores to 20 kbar together with melting data and thermodynamic parameters used in the calculation.

2. Pressure Studies of the Fermi Surface of Thallium
AEC, ARPA (Anderson)

The Fermi surface of thallium has been investigated at normal pressure and as a function of pressure (with the fluid helium phase shift technique) by using the de Haas-van Alphen (dHvA) effect to measure extremal cross-sectional areas. The frequencies observed by Priestly using pulsed magnetic fields, were measured more accurately with the aid of NMR calibrated superconducting and iron magnets. In addition, several new low frequencies were observed in the range from 2×10^5 to 5×10^6 Gauss. The logarithmic pressure derivatives of these frequencies range from $0.13\%/\text{kbar}$ to $1.6\%/\text{kbar}$. The latter value is about 9 times the compressibility scaling prediction neglecting any change in the c/a ratio. The normal pressure Fermi surface has been mapped out by studying the orientation dependence of the dHvA oscillations. The dHvA frequencies and logarithmic pressure derivatives will be compared with calculations based on the Heine-Abarenkov model potential.

3. IR Dichroism Study of Polyethylene Crystallized under the Orientation and Pressure Effects of a Pressure Capillary Viscometer
NSF (Jackson)

Polarized infrared spectra have been obtained on a Digilab FTS-14 Interferometer of a sample of the transparent polyethylene in the frequency range from 450 to 3500 cm^{-1} . The

transparency of these polyethylene filaments is known by x-ray to be associated with high crystal orientation along the filament axis. Use of appropriate thickness of the tiny sample has allowed 2 cm^{-1} resolution at reasonable intensities for bands of widely different magnitudes. Analysis of the purely crystalline absorptions shows that the c axis of the orthorhombic unit cell is essentially perfectly oriented in the long direction of the transparent rod, i.e., in the direction of extrusion during formation. Comparison of the dichroism of the absorptions due to noncrystalline regions with earlier dichroic studies of drawn polyethylene films indicates that the amorphous region, while showing low orientation, does exhibit dichroism similar to stretched films of draw ratio between $\lambda=2$ and $\lambda=7$. Bands known to contain both amorphous and crystalline components exhibit dichroism consistent with the relative proportions of crystalline and amorphous material calculated using the techniques of Okada and Mandelkern. These values, $86 \pm 3\%$, are comparable to values estimated from direct density measurement. The spectra thus may be used to differentiate between absorptions due to purely crystalline and purely amorphous components as well as those due to combinations.

4. Direct Microscopic Observation of the Crystallization Process of Polyethylene at High Pressure: Acicular or Bladed Crystals

ARPA

(Jackson & Brasch)

It has been known for some time that fracture surface replicas of high pressure crystallized polyethylene exhibit unusual, large structural features of the crystalline polymer when viewed by transmission electron microscopy.

These studies show regions of order in the fracture surface with dimensions in the range 1000\AA to 1.1 microns. Fracture surfaces of polyethylene crystallized at atmospheric pressure show lamellar structures which exhibit the smaller dimensions of the order of one thousand angstroms, but in these cases the higher order dimensions are not well defined.

Numerous thermodynamic studies of high pressure polyethylene crystals have been carried out. However, few studies of the actual high pressure crystallization process have been reported. In only two cases have optical microscopic investigations been reported, and both of these have reported presence of spherulitic structures in the high pressure crystallized material.

This letter is a preliminary report of direct observation by birefringence microscopy of the actual crystallization process which takes place in polyethylene at high pressure and temperature in a high pressure diamond cell.

C. PHASE TRANSITIONS AND CRITICAL PHENOMENA

1. Neutron Scattering Study of the Lattice Dynamical Phase Transitions in KMnF₃ (Minkiewicz)
ARPA

Neutron scattering experiments have been carried out to study in detail the characteristics of the structural phase transitions in KMnF₃ at 186.6°K and 91.5°K. The two transitions are known to be caused by soft phonon mode condensation at the [111] and [110] zone boundaries, respectively. The temperature dependence of the intensity of the superlattice Bragg reflections displays a small but definite discontinuity at the 186.6°K transition and shows typical first order behavior at the 91.5°K transition. At both transitions, however, the soft phonon mode intensities diverge in a manner that is typical of a second order phase transition.

2. Superconductivity of Beryllium Films (Glover)
Deutsche Forschungsgemeinschaft

Beryllium films condensed on liquid helium cooled substrates were found to be superconducting in agreement with earlier work. A transition temperature of 9.6°K, about a degree higher than found previously, was indicated by a rapid drop in resistance with cooling. Various experimental checks show that this behavior is characteristic of pure beryllium.

3. Effect of Surface Charge on the Superconducting Transition Temperature and Normal-State Conductivity of Disordered Metal Films (Glover)
Deutsche Forschungsgemeinschaft

Measurements were made of the shifts with added electrostatic charge of the normal-state residual conductivity and superconducting transition temperature of films of amorphous Bi and Ga, metastable crystalline Ga, and disordered crystalline Pb. For the amorphous Bi samples adding electrons increased both the superconducting transition temperature, T_c, and the residual conductivity, σ. For the other materials adding electrons lowered both T_c and σ. In each case removing electrons produced a shift of equal magnitude but of opposite sign to that observed for negative charging. For a given applied charge the shifts in T_c and σ were proportional to the reciprocal of the film thick-

ness within the accuracy of the measurements. Results were reproducible from sample to sample. The correlation between the signs of the shifts in T_c and σ for the metals investigated was the reverse of that observed previously for Sn, In, and Tl. Measurements were also made of the effect of condensed oxygen on the superconducting transition temperature of the films. Physically adsorbed oxygen lowered T_c for all of the materials. Increasing the temperature to the point that a reaction between the metal and the condensed oxygen began produced a further reduction in T_c for Pb and metastable crystalline Cu.

4. Depression of T_λ by a Heat Current (Bhagat)
ARPA

Earlier experiments on the HeII-HeI transition in a heat current have been repeated in several different flow geometries in an attempt to discover the reason for discrepancies among various observers. Detailed analysis of the data has allowed us to suggest a mechanism which may account for the apparent inconsistencies.

5. The Velocity of Second Sound in a Heat Current (Bhagat)
ARPA

Preliminary measurements on the variation of the speed of second sound in a heat current, Q , are reported. It is found that at temperatures close to T_λ , u_2 reduces quadratically with Q , for small Q .

6. HeII-HeI Transition in a Heat Current:
Model Calculations (Bhagat)
ARPA

The Ginzburg-Pitaevskii phenomenological theory had been extended to include the effects of vortex lines. The model calculations are compared with some of our recent experimental results on the HeII-HeI transition in the presence of a heat current.

7. Photon Counting, Correlation Functions, and the
Critical Region (Korenman)
ONR

The statistical distribution of the number of photoelectrons emitted in a short time interval from a phototube illuminated by laser light scattered from a fluid is examined. Moments of this distribution measure correlated scattering of photons and are related to

density correlations of various orders in the fluid. It is pointed out that a measurement of the second moment will indicate whether corrections are needed to the usual interpretation of the scattered-light spectrum. Deviations of the higher moments from the value for uncorrelated scattering would allow measurement of the spatial dependence of multiparticle correlations. The strength of the correlated scattering contribution to the various moments is estimated near a critical point, where it is expected to be largest, using a scaling-law equation of state and available data for simple fluids. According to this estimate, measurement of these multiparticle correlations will be very difficult in a simple fluid. It is pointed out that it may be easier near the critical mixing point of a binary fluid.

8. Rayleigh Scattering Near the Critical Mixing Point of 3-Methyl-Pentane-Nitroethane (Sengers & Alley)
ARPA, ONR

The Rayleigh linewidth for the binary liquid 3-methyl-pentane-nitroethane has been measured as a function of temperature. The data encompass scattering angles from 40° to 130° and cover a range of .1 to 20 in the scaling parameter $k\xi$. We have used a helium-neon laser as the light source and have employed the self-beating technique developed by Benedek. Our data agree well with dynamical scaling predictions. In particular, we have accurately confirmed the predicted k dependence of the linewidth for $k\xi \gg 1$. Comparison with the more detailed predictions of Kawasaki and Ferrell will also be made.

9. Decoupled-Mode Dynamical Scaling Theory of the Ferromagnetic Phase Transition (Ferrell)
NSF, ONR, AFOSR

The dynamical scaling theory of phase transitions begins below the phase transition and extrapolates the frequencies, by means of the temperature continuity at a finite wave number, through the critical point into the temperature region above the transition. Applied to the ferromagnet, this approach leads to the observed five-halves critical dispersion at the Curie point. In the paramagnetic region it yields the critical slowing down of spin diffusion with a critical exponent of one-third. An alternative approach beginning in the paramagnetic region has been developed from the basic statistical mechanics of spin interaction. In the present paper, we present a simplified version of this approach, based on the fluctuation-dissipation theorem. The relevant form of this theorem is easily derived along familiar lines and involves obtaining an expression for the spin current. The spin diffusion coefficient is then expressed in terms of the ratio of the fluctuations in spin current and spin density. The correlation function

for the current fluctuations can be evaluated by factoring (decoupled-mode approximation). The results are shown to be equivalent of those obtained by the other methods, and a simple explanation is given for the rise of the scaling function outside of the hydrodynamic region.

10. Decoupled-Mode Dynamical Scaling Theory of the Binary-Liquid Phase Transitions

AFOSR, ONR, NSF

(Ferrelli)

The critical slowing down of the diffusion in a binary liquid is calculated from the fluctuation-dissipation theorem. The fluctuating current is the product of the local fluctuations in concentration and velocity. Assuming statistical independence of these variables yields results identical to those found by Kawasaki using another method.

11. Scaling of the Thermal Conductivity Near the Gas-Liquid Critical Point

ARPA, ONR

(Sengers)

The thermal conductivity of a gas becomes infinite at the critical point. It is shown that the experimental data for the thermal conductivity of CO₂ satisfy scaling-law relations very similar to those previously established for equilibrium properties near the critical point. The analysis also suggests that the values reported in the literature for the critical exponent of the Rayleigh line width should be revised downwards.

12. On the Density Expansion for Viscosity in Gases

NSF, AEDC, NBS

(Sengers)

Results are presented of new, precise measurements of the viscosity of nitrogen, argon, and helium at 25°C. The measurements were performed over a nominal range of pressures 1-100 atm and at very closely spaced density intervals. The data were subjected to a stringent statistical analysis in order to determine whether the density expansion consists of a pure polynomial or whether a term of the form $\rho^{\alpha} \ln \rho$ must be included in it. The existence of such a term was discovered theoretically by several investigators. The analysis indicates that if such a term exists, its factor must be very small. Moreover, the statistically significant interval of values which this factor can assume includes zero in it.

This result is interpreted as indicating that correlations which extend over distances of the order of a mean free path are negligible when compared with correlations which extend over distances of the order of the range of molecular interactions.

13. Three-Particle Collisions in a Gas of Hard Spheres
AEDC (Sengers)

The triple-collision integrals which determine the first density correction to the transport coefficients are derived for a gas of hard spheres using the binary-collision expansion. This expansion provides a convenient technique for classifying the contributions in terms of sequences of successive binary collisions between three molecules. Such sequences contain both interacting and noninteracting collisions. It is demonstrated that for three hard spheres all sequences terminate after four successive collisions, independent of the interacting or noninteracting nature of the collisions. As a consequence, the collision integrals are related to a limited number of sequences with three and four collisions only. It is shown that equivalent results are obtained from the surface-integral form of the triple-collision operator, derived earlier by Green and Sengers.

D. RADIATION EFFECTS ON MATERIALS

1. Berg-Barrett X-ray Observation of Annealing and Laser Induced Damage in Zinc
ARPA

(Lee & Armstrong)

The Berg-Barrett X-ray diffraction contrast technique has been utilized to study the process of laser induced damage in a zinc crystal and, also to make observations on the annealing characteristics of the dislocation substructure before and after the laser treatment. Annealing caused individual dislocations to become segmented with various sections of their line lengths becoming parallel to $\langle 10\bar{1}0 \rangle$. This preference for a crystallographic orientation of the dislocations seemed related to the equally important observation that the subboundary "lineage" structure of the crystals was also largely composed of tilt boundaries of $\{10\bar{1}0\}$ and $\{11\bar{2}0\}$ surfaces. The laser induced damage required a threshold energy which caused melting, possible vaporization and appreciable plastic deformation of the matrix material by deformation twinning, non-basal slip and micro-kinking. By comparison with the structural rearrangement observed in the pre-annealed specimen, the laser damage zone showed only very retarded changes.

2. A Dynamic Dislocation Pile-up in Neutron-Irradiated Metals
AEC

(Arsenault)

The formation of a dislocation pile-up was examined for the condition where there is a finite removal probability of the short-range barriers (s.r.b.) to dislocation motion. The purpose of investigating this type of dynamic pile-up formation was to determine whether the rapid rate of slip-line formation in neutron-irradiated metals could be a thermally activated process. The evidence obtained affirms the possibility of having slip lines form rapidly while the process is still thermally activated.

3. Low Temperature Deformation Characteristics of Neutron Irradiated Vanadium-Titanium Alloys
AEC

(Arsenault)

An investigation was undertaken to determine the effect of neutron irradiation on the low temperature deformation characteristics of vanadium-titanium alloys. The effect can be divided into two groups: for low titanium concentrations (0.75 and 1.6 wt. per cent Ti) a weakening effect appeared which was apparent for the complete temperature range investigated for the 0.75 percent Ti but to a lesser extent for the 1.6 per cent titanium alloy. For alloys with higher titanium concentration (4-20 percent Ti), the neutron irradiation does not effect the thermal component of the yield stress, i.e.

no change in the rate-controlling mechanism of low temperature deformation occurs. For both alloy groups the neutron damage resulted in an increase in the athermal component of the yield stress.

4. Melting Behavior of Radiation Crosslinked Crystals of Polyethylene

Res. Corp.

(Jackson)

The melting behavior of polymer crystals crosslinked in the ordered, crystalline state is expected to be a complicated function of the effects of crosslinking on the relative entropies of the crystal-amorphous mixture, on the one hand, and the amorphous melt on the other. Flory has shown that one effect of crosslinking is to increase the entropy of the melt in a manner analogous to copolymerization, leading to a decrease in melting temperature. However, crosslinks formed adjacent to the axially ordered crystalline phase should result in maintenance of some degree of order in the liquid phase and a decrease in configurational entropy of the chains in the melt, resulting in an increase in melting temperature. Mandelkern, *et al*, have shown that polyethylene crosslinked in the molten state shows a large depression of melting point after subsequent crystallization. The depression observed is a function of fraction of cross-linked units but is larger than expected on the basis of entropy effects. This results from decreasing size of the crystallites formed. Networks formed in the fibrous or axially oriented state also showed a decrease in melting temperature of the isotropically crystallized resultant network, but the depression was significantly less than that observed when molten polymer was crosslinked.

Since kinetic effects are predominant in the melting of dilute solution crystals, differential scanning calorimetry affords a good technique for investigating the nature of these changes. However, the important thermodynamic parameters, with the exception of enthalpy, such as melting point and dissolution temperature are better studied by other techniques. The purpose of the present study was to examine the effect of radiation crosslinking on melting and recrystallization processes of dilute solution crystallized polyethylene crystals.

5. The Application of Radiochromic Dye Film Dosimetry to Medium-Z Absorbers

AEC; NBS

(Silverman)

The use of radiochromic dye films for electron dosimetry was extended to absorbers with atomic numbers in the range 12 to 50. The depth-dose profiles in slab targets of aluminum, copper, and tin irradiated by 2.00 MeV electrons with the incident beam at 0, 30, and 60 degrees to the

surface normal were determined using calibrated films and simultaneous charge measurements. The results are compared to the ionization measurements of Nakai where appropriate, and to theoretical calculations by the ETRAN code, and agree within $\pm 5\%$. The stopping power correction necessary to convert dose in the film to dose in the absorber was made (1) by computer calculation, averaging over the spectrum present at each depth of interest, (2) by evaluating the ratio at each depth at the mean energy of the spectrum calculated from a simple, empirical formula, and (3) by selecting an average stopping power ratio independent of energy. The three methods yielded dose-depth profiles which agreed within $\pm 3\%$ over most of the range.

6. Radiation Induced Polymerization of Pure Styrene at Low Temperature

AEC

(Silverman)

The radiation induced polymerization of styrene was carried out over a range of temperature from 0 to 78°C using superdry styrene and wet styrene. Molecular weight distributions were determined by gel permeation chromatography. In the course of the rate studies, the time of contact between styrene and silica gel was found to be an important factor. Partially dried liquid styrene shows a bimodal molecular weight distribution which reflects the simultaneous operation of ionic and radical processes. Upon solidification, superdry styrene exhibits a sharply decreased rate of polymerization, while wet styrene shows a marked increase. The polymer from superdry styrene shows a unimodal molecular weight distribution when formed in the liquid phase, and a multimodal distribution when polymerized as a solid. At -78°C , the rate of polymerization and the molecular weight of the product are rather low. In a sample irradiated at -78°C and then stored at the freezing point of styrene (-30.5°C) for a few hours, the polymer yield shows a large increase accompanied by the appearance of a very high molecular weight fraction in the distribution curve. Traces of water have no effect on the rate of polymerization and molecular weight distribution of frozen samples. A high yield of dimer and trimer, $G \approx 2.5$, is observed in wet liquid styrene. This can be attributed either to intraspur radical reactions or to water terminated ionic reaction in the bulk phase. The results in the solid state polymerization fit the assumption that a carbonium ion propagation predominates regardless of the water content.

7. Short-Lived Transient Species in Irradiated n-Hexane
AEC; DASA (Silverman)

We have observed the transient electrical conductance in n-hexane at times ranging from 25 nsec to 2 msec after a 25 nsec pulse of bremsstrahlung. As an improvement over prior methods, our technique allows the observation of both the second-order recombination as well as early first-order trapping. This enables us to report the lifetime and mobility of a new fast carrier as well as the G value and ratio of recombination coefficient to mobility, k/u, for the latter species, all taken on the same sample.

8. Effect of Swelling on Radiation-Induced Grafting of Styrene to Polyethylene
AEC (Silverman)

The radiation-induced grafting of low-density polyethylene in contact with styrene solution was studied. The effect of the degree of swelling of the polymer on the rate of grafting was investigated by diluting the styrene with methanol and with n-octane. For styrene-methanol solution, the rate of grafting was found to increase with degree of swelling, passing through a maximum when the sorbed solvent reaches 6.2 wt-% (70 vol-% methanol in the outside solution) and decreasing thereafter. The methanol fraction of the sorbed liquid is far too small to cause precipitation of the grafted chains and inhibition of their termination rate. The dilution of styrene by octane has no effect on the swelling of polyethylene, but it decreases the grafting rate over the entire concentration range. The results are explained in terms of the concentration of sorbed monomer and the viscosity of the amorphous region of the polyethylene swollen by non-polar liquids. Supporting evidence for the mechanism is presented in the form of grafting kinetic data as a function of dose rate (2.8×10^2 - 9.5×10^4 rad/hr), and post irradiation grafting measurements for polyethylene in methanol-styrene (70/30, v/v). The data indicates that at the maximum grafting rate an optimum is achieved between a high concentration of sorbed monomer and a low viscosity for the poorly swelled polymer matrix.

9. Dose-Depth Distributions Produced by Electrons in Multi-Layer Targets
AEC (Silverman)

The purpose of this study is to solve a series of practical problems involving the use of electron beam and beta sources for radiation processing applications. Monte Carlo computations were performed to determine the energy absorption, reflection and transmission for the following configurations: plane parallel source of mono-energetic electrons incident on one face of a slab of a multi-layered target; planar and line sources with electrons incident on cylindrical

targets. The slab calculations were performed as a function of target composition (water, iron and polyethylene), thickness of the individual layers, electron energy (0.1, 1.0 and 10.0 MeV) and angle of incidence between the electrons and the normal slab (0° , 30° , 60° , and 90°). The cylindrical calculations were performed on finite and infinite cylinders. The method used is similar to the one employed by Berger in his calculations of dose-depth curves in semi-infinite slabs. It takes into account energy losses from collisions with atomic electrons based on the continuous slowing-down model; it assumes a net angular deflection at the end of each selected path length on the basis of the multiple scattering elastic theory of Goudsmit and Saunderson; and it employs a mean bremsstrahlung energy loss over each path length. The principal information derived from the study is the distribution of energy dissipated within the target as a function of position for target systems of practical interest to the radiation processor and principles for the most efficient utilization of electron beam sources.

E. MECHANICAL PROPERTIES OF MATERIALS

1. Unusual Fracture Features of Oxidized Vanadium +1.31 at .% Titanium Alloy
AEC (Arsenault)

Fractography of a b.c.c solid solution vanadium +1.31 at .% titanium alloy has been examined by a scanning electron microscope (SEM). In this alloy titanium acts as a scavenger of interstitial impurities. Specimens in the annealed--"as received" condition and with oxygen concentrations of 0.083 and 1.14 at .% were fractured to observe the fracture morphology. The fracture morphology of the two specimens containing a large oxygen concentration had geometrically faceted fracture surfaces and the presence of oxides was not found in the fracture features. Metallographic analysis showed the existence of oxide precipitates, and an explanation is advanced as to the differences in the SEM and metallographic results.
2. Alloy Strengthening Due to Atomic Order
AEC, AMES LAB (Marcinkowski)

Compressive stress-strain curves have been obtained for a large number of metals and alloys in both the ordered and disordered configurations. The deformation behavior of these materials can be rationalized in terms of three distinct stages. Each of these stages has been accounted for in terms of the dislocation configuration existing in the particular material.
3. Twist Boundaries in Ordered Alloys
AEC (Marcinkowski)

A detailed analysis has been made of the equilibrium configuration of some of the simpler types of twist boundaries anticipated in ordered alloys. Similar to the case of tilt boundaries, it is found that the extension of the superlattice dislocations decreases with increasing angle of misfit of the boundary. Furthermore, at sufficiently high angle, the boundary becomes completely disordered. An examination of twist boundaries in ordered FeCo shows them to consist of superlattice dislocations in all cases, but somewhat more complex than those treated theoretically and described above.

4. Dislocation Behavior at Grain Boundaries under Heterogeneous Shear

NSF

(Marcinkowski)

The heterogeneous shear of grain boundaries by the passage of a number of glide dislocations on a single slip plane from one grain to the adjacent grain across the grain boundary has been studied. The resulting stress field was determined by treating the disturbance left at the boundary after the passage of glide dislocations using the concept of virtual dislocations. Depending on whether the virtual dislocation is mobile or not in the grain boundary plane, it is shown that heterogeneous shear of grain boundaries can produce grain boundary sliding, grain boundary ledges or may act as a precursor to crack initiation.

As was done in the case of homogeneous shear of grain boundaries, the present study is carried out for several simple cases involving symmetric tilt and twist boundaries. Screw and edge dislocations are treated separately.

5. Thermal Microstresses in Beryllium and other HCP Materials

AEC

(Armstrong)

The thermal stresses that may develop due to crystal anisotropy within the microstructure of beryllium and certain other hcp materials are described. The magnitude of the unrelaxed thermal stress in polycrystalline beryllium is estimated numerically. The calculated values for the local thermal stresses that might occur in polycrystalline beryllium are comparable to the bulk stresses that are measured for yielding and fracture. The possible influence of these stresses on the initiation of cleavage cracks in rolled beryllium sheet and in extruded beryllium plate is described.

6. Total Material Variables Influencing a Ductile-Brittle Transition Temperature for Molybdenum

ARPA, ONR

(Armstrong)

The ductile-brittle transition temperature for a coarse grained recrystallized molybdenum material was found to be lower than for the original fine grained metal from which it was produced. The coarse grain size resulted from a critical straining and subsequent annealing treatment at a low recrystallization temperature. It is concluded from an analysis of various strength parameters which are either measured or estimated for this material that an improved grain boundary strength and a considerable influence of the dislocation substructure are responsible for the less brittle behavior of the coarse grained molybdenum.

7. Determination of the Frictional Stress for Polycrystalline Iron and Carbon Steels from their Stress-Strain Behavior and its Grain-Size Dependence

AEC

(Armstrong)

Two improved procedures involving extrapolation of both the grain size and plastic strain are developed to determine the frictional stress at zero plastic strain in polycrystalline iron and mild steels. The procedures for these extrapolations are based on two newly observed experimental relations: (1) The Petch parameter σ_f satisfies the Ludwik equation, and (2) the stress term obtained from the plastic-strain extrapolation of a single stress-strain curve is proportional to the reciprocal of the grain size. Both methods yield the same limiting frictional stress of 5.2×10^3 lb/in². This value is in excellent agreement with experimental results reported for single crystals and polycrystals.

8. Fracture of Bone Materials in Compression at Temperatures between -200°C and +200°C

ARPA, ONR

(Armstrong)

Recent studies of bone materials have suggested that the fracture behavior is sensitively dependent on specimen orientation, microstructure, the presence of external notches, temperature and the deformation rate imposed. The deformation properties of bone have been likened to those expected of composite materials. This study provides further information about the strength of bone and helps to define the criteria which must be satisfied by theoretical models of the mechanical properties.

9. Solute-Subgrain Boundary Interaction in Niobium

ARPA, AEC

(Armstrong)

Recently the subgrain size dependence of the critical resolved shear stress, τ_{CRSS} , for electron beam float zone refined niobium single crystals has been shown to follow a Hall-Petch type of relation, as follows

$$\tau_{CRSS} = \tau_0 + k_s l_s^{-1/2}$$

where l_s is the average minimum subgrain size measured along the diameter of the crystal cross-section, and τ_0 and k_s are experimental constants. This relation has been proposed by a number of investigators to describe their own experimental results and, also, other previously uncorrelated results have been fitted to it. In the case of niobium, however, an exceptional microhardness of the subgrain boundaries, comparable to the maximum value measured for grain boundaries of niobium polycrystals,

was also reported. The value of k has been favorably compared with other recent measurements of the polycrystal hardness dependence on grain size. It was predicted from the last-mentioned comparison that the "true" polycrystal k value for the yield stress dependence on grain size or subgrain size was near to $1.1 \text{ kg/mm}^{3/2}$. A connection has been shown between the foregoing results and analysis and those results which have been reported by Omar and Entwistle.

10. The Critical Resolved Shearing Stress of a Silver 2.9% Indium Alloy as a Function of Growth Rate

AEC

(Asimow)

The critical resolved shearing stress of Ag-2.9at.% In was measured as a function of crystal growth rate and of tensile test temperature. The growth conditions were such that microsegregation is anticipated. It was found that the growth rate has a negligible effect on the thermal stress component but a significant effect on the athermal stress component. It is suggested that the increase in athermal stress is related to the formation of substructure with boundaries of high dislocation density. A method of extrapolation of the athermal component to subcritical growth velocities is given.

F. DEVICE TECHNOLOGY

1. Relative Frequency Stability of Stable He-Ne Gas Laser Structures

ONR, ARPA

(Hochuli)

Enhanced He-Ne gas laser stability has been achieved by constructing the mirror and gas discharge tube as an integral unit. The primary components are made from Corning ULE and 99JJW ultralow thermal expansion materials; ultrahigh-vacuum type materials are used throughout. The ambient pressure sensitivity of these 6328Å laser structures is 2.5 MHz/torr. Preliminary beat frequency measurements between two lasers, under pressure and temperature-controlled conditions, have yielded a beat frequency spectral width of the order of 2kHz over an interval of 1s. This result was achieved without the use of any elaborate sound or vibration isolation. Improved isolation reduced the spectral width to 100Hz for a measurement duration of 0.02s. The single-structure mirror-discharge tube has provided relative output power stabilities of better than 3 parts in 1000 over a period of 12h. The frequency modulation sensitivity is 1.2 kHz/ μ A of discharge current, from dc to 100 kHz.

2. CO₂ Laser Life Study

NASA

(Hochuli)

As originally proposed, we have searched for methods to extend the lifetimes of sealed-off CO₂ lasers. We began by investigating various cathode materials under gas discharge conditions in Pyrex envelopes. Only clean metal to glass seals were made to the envelope. No epoxy resin was ever used.

Over twenty electrode materials in more than 70 discharge tubes were tried, most of which turned out to be unsatisfactory. The materials tested were: Ti, Ta, Be, Al, Au, Pt, Pd, Ir, Co, Cd, Mn, Mn-Cn-Ni alloys, TiC, TaC, NbC, WC, HfC, TiD₂, ZrB₂, LaB₆, and a TiC + NbC cermet with a Ni binder. Only the last material showed a consistently better sputtering resistance. To avoid duplicating the work of others, and because this cathode is expected to out perform nickel cathodes at lower temperatures, we concentrated our following efforts on this material. We do, however, have to admit that the materials we abandoned are not necessarily unfit. There are simply too many parameters involved all of which could not be tested. To support this argument we have only to mention that the nickel cathode is not particularly successful until it is heated above 200°C.

3. Comparison of Input Offset Voltage of Differential Amplifiers Using Bipolar Transistors and Field-Effect Transistors

(Lin)

For most differential amplifiers intended for dc operations, it is desirable to have high differential input resistance to minimize the loading of the source generator. Bipolar transistors have relative low input impedance. By operating the input stage at low collector currents and/or using Darlington input stages, differential input stages of the order of 10^5 ohms have been achieved. A field-effect transistor (whether junction type or MOS type) has very high input impedance. For those who desire to achieve a higher input impedance, it is often asked "Why aren't FET pairs used as input stages and bipolar transistors used as output stages, since compatible FET and bipolar transistor monolithic structures have been developed?" This correspondence is a study of this question.

4. Silicon Contact for Area Reduction of Integrated Circuits

NASA

(Lin)

The area of integrated circuits can be reduced by not allowing any space between the contact and the junction edge. Epitaxially grown silicon contacts have been used to achieve this goal.

5. Bi₂Se₃ Hall Effect Magnetometer

AEC, ARPA

(Spain)

Bi₂Se₃ grown by the Bridgman technique is found to make an excellant Hall effect magnetometer. Plots of Hall resistivity, ρ_{xy} , vs magnetic field, H, to 8 tesla are linear to within one percent. The slope of the ρ_{xy} vs H curve varies by about one percent in the region 4K to 35K and by only twenty percent in the region 4K to 300K.

Analysis of galvanomagnetic and optical absorption measurements indicate the samples behave as semimetals with at least two band conduction.

6. Voltage-frequency Converter uses Four-Layer Diode

(O'Haver)

By using a four-layer diode to reset a conventional dc integrator to a fixed potential, a voltage-to-frequency converter (or voltage-controlled oscillator) can be built with only one operational amplifier and four other components. The circuit offers a conversion linearity of better than $\pm 0.2\%$ of full scale from 0 to 10 volts. In addition, both sawtooth and pulse outputs are available.

7. The Application of Field-Effect Transistors as Precision
Analog Switches in Laboratory Instrumentation
ARPA (O'Haver)

Junction field-effect transistors (FET's) used as analog switching elements in laboratory instrumentation provide high performance, economy, and circuit simplicity. An error analysis and some criteria for selection of FET types are given. FET analog switches are particularly suitable for use in operational amplifier circuits. Several useful applications to laboratory instrumentation are discussed.

S. SYNTHESIS, STRUCTURE AND REACTIONS OF MATERIALS

1. Tertiary Phosphine Complexes of Rhodium(III) and Rhodium(I)

AFOSR

(Grim)

Phosphorus-31 magnetic resonance spectra are reported for twelve compounds of the type $\text{mer-}[\text{R}_n\text{Ph}_{3-n}\text{P}]_3\text{RhCl}_3$, where R is alkyl and n is 1, 2, or 3. The rhodium-103-phosphorus-31 coupling constant is always larger for a phosphine trans to another phosphorus. Coupling between the non-equivalent phosphorus nuclei is also observed. Virtual coupling in the proton magnetic resonance spectra of methyl- and ethyl-phosphine complexes is examined. Visible-ultraviolet spectra are presented.

2. A Phosphorus-31 Magnetic Resonance Study of Tertiary Phosphine Palladium(II) Compounds

AFOSR

(Grim)

Phosphorus-31 chemical shifts are reported for thirty-one compounds of the type, cis-- and trans-- L_2PdCl_2 , sym-- $\text{L}_2\text{Pd}_2\text{Cl}_4$ and trans-- $\text{L}(\text{Am})\text{PdCl}_2$, where L is a tertiary phosphine and Am is a nitrogen ligand. Many of the compounds are previously unreported. For a particular phosphine ligand the chemical shift of the cis isomer is down-field from that of the trans isomer. Some infrared frequencies and proton nmr results are also given.

3. Preparation of 2-diphenylphosphinoethylphosphinites

NSF

(Grim)

In an extension of studies of the synthesis of chelating bis-phosphorus ligands which have chemically non-equivalent phosphorus atoms, two compounds of the type $\text{Ph}_2\text{PCH}_2\text{CH}_2\text{OPR}_2$ where R is phenyl or butyl, have been prepared. These compounds have potential importance as ligands for ^{31}P magnetic resonance studies of coordination compounds because of the possibility of observing phosphorus-phosphorus coupling directly in the ^{31}P spectra of the complexes.

4. Bond Angles, Hybridization and Phosphorus-Metal Bonding

NSF

(Grim)

A method of calculation is described whereby the s-character of each of the four hybrid orbitals of the central atom of a distorted tetrahedron is determined from the six unique bond angles. The method is applied to several simple molecules and to some phosphorus coordination compounds. It is demonstrated that s-character of the

bond is not necessarily the major factor in determining the magnitude of the phosphorus-heavy metal spin-spin coupling constant in these coordination compounds.

5. Upfield and Downfield Shifts in the Nuclear Magnetic Resonance Spectrum of a Tris(Dipivalomethanato) Europium(III) Complex

ARPA

(Mazzocchi & Miller)

In the course of a photochemical investigation, a product was isolated whose nmr spectrum was difficult to interpret due to coincidences in the chemical shifts of a number of its protons. Treatment of the product with Eu(DPM)₃ caused chemical shift changes sufficient to allow the analysis of the proton spin-spin couplings on a first order basis. Decoupling experiments confirmed the proton assignments and the structure.

6. The Photoisomerization of 2-Cyclopropyl-1-phenylethylene
Res. Corp. (Mazzocchi)

The photoisomerizations of several vinylcyclopropanes to cyclopentenes have been described and their photochemical reactivity roughly correlated with their ground state conformation.

7. Thermodynamic Equilibria from Plasma Sources. Carbon-Hydrogen-Nitrogen Systems

NASA

(Lippincott)

Some organic nitrogen compounds have been subjected to a radio-frequency electrodeless discharge, and the products analyzed. Although the exact composition can be explained only by invoking kinetic factors, the approximate product distribution as the species emerge from the plasma may be computed by assuming a high-temperature limited thermodynamic equilibrium. The final distribution of the hydrocarbons corresponds to a temperature of about 1300°K, while that of the major nitrogenous compounds corresponds to a higher temperature, owing to the high activation energy needed to break the triple bond of the cyano radical which is formed in the plasma.

8. Reactions of Diboron Tetrahalides with Haloolefins.

Formation of Poly(Dihaloboryl)ethanes.

ARPA

(Bellama)

Tetrachlorodiborane reacts with vinylchloride in 2/1 ratio to yield 1,1,2-tris(dichloroborylethane and boron trichloride. The reaction appears to be general for a variety of haloolefins. Both B_2Cl_4 and B_2F_4 react similarly with haloethylenes containing halogens heavier than the halogen on the diboron moiety. Evidence has been obtained for a reaction sequence involving addition of B_2X_4 to the haloolefin, elimination of trihaloborane, and subsequent addition of B_2X_4 to the resulting vinyl-dihaloborane.

9. Mechanisms for the Thermal Decomposition of Polyethylene

Goodyear Tire Co.

(Bailey)

Since previous work on the mechanism of the thermal decomposition of polypropylene, polyisobutylene, and polystyrene showed that the products from the pyrolysis vary considerably with the conditions of the decomposition and that very often cyclic processes, both radical and molecular, were important, study of the mechanisms of the thermal decomposition of polyethylene was undertaken. Many workers usually cite polyethylene as an example of a polymer which does not yield a monomer to any appreciable extent upon decomposition. However, practically all previous workers studied the decomposition below 500°, under which conditions they report that the decomposition is extremely complex. In contrast, we found that the decompositon of polyethylene at 600° gives essentially only four major volatile products and 60% of the volatile material consisted of monomeric ethylene. The other major products were ethane, propane and propylene. In agreement with previous work, however, at 415° eleven major volatile products were produced in which the predominate component was propylene and the presence of very little ethylene was noted. Although it was possible to rationalize the formation of the various products produced in the decomposition it was considered desirable to collect additional evidence for the mechanism of their formation. Considerable evidence for the mechanisms of several products was established by the thermal degradation of a regular alternating copolymer of ethylene and deuteroethylene. The formation of several of the volatile products, such as ethylene and 1-pentene, could be best explained by a process involving only intramolecular mechanisms. Other products, such as ethane and 1-pentene, could be best explained by a process involving only intramolecular mechanisms. Other products, such as ethane and propane, were best rationalized by a process that involved at least one intermolecular process. Some products, such as propylene, could be rationalized either on the basis of an intramolecular process or an intermolecular process. In order to distinguish between these various possibilities and to establish whether the formation of any given product involved an inter- or intramolecular process, it was of interest to study the decomposition of polyethylene with the aid of deuterium tagging.

10. A Convenient Preparation of Cyclohexane-1,4-dicarbaldehyde
and Cyclohexane-1,1,4,4,-tetramethanol
ARO (Bailey)

1,4-Bis(allyloxymethyl)cyclohexane was pyrolysed at 540-545° to give primarily cyclohexane-1,4-dicarbaldehyde, which, after a Tollens reaction, gave cyclohexane-1,1,4,4-tetramethanol.

11. New Spiro Polymers Containing Five-, Six-, Seven-, and
Eight-Membered Cyclic Metals
Goodyear Tire Co., ARO (Bailey)

Spiro polymers, which are double-stranded polymers, have attracted interest because they have extremely high melting points because of restricted rotation and have a high degree of chemical and thermal stability since they are resistant to changes in molecular weight. The first organic completely spiro polymer was recorded by Bailey and Volpe by the condensation of pentaerythritol with 1,4-cyclohexanedione. This material, although soluble in hexafluoroisopropanol, did not melt and was more thermally stable than corresponding open-chain polyethers. This type of synthesis was extended to a series of sulfur-containing spiro polymers which were prepared from pentaerythrityl tetrathiol and cyclic diketones. These materials, although insoluble in all solvents tested could be oxidized to soluble polysulfoxides and polysulfones. A number of other spiro polymers have been reported recently including polyspiro-benzothiazolines, the condensation products of dianhydrides with tetraamines, spiro polyallenes, and spiro tetrasulfides.

It was of interest to extend the reactions of tetrols with cyclic diketones to produce a variety of spiro polymers with less oxygen in the base chain and with other functional groups present in the molecule. Therefore the synthesis of a number of tetrols which would be useful in preparing polyspiroketal was undertaken. For this reason, 1,1,4,4-tetrakis-(hydroxymethyl)-cyclohexane was prepared by a sequence of reactions, and condensed with the tetrakis-cyclohexanone to produce an 80% yield of the model spiro ketal. Under very similar conditions, then, the tetrol plus 1,4-cyclohexanedione was condensed to produce a 70% yield of the corresponding polyspiroketal.

12. A Degradation Study of Some Formaldehyde-Modified Celluloses
Cornell Univ. (Agric. Exp. Sta.) (B. Smith)

The chemical and physical properties of cotton fabrics treated with formaldehyde in the presence of an acid

catalyst (HCl) under aqueous (Form W) and essentially nonaqueous (Form D) conditions were investigated. Physical properties (tear strength, breaking strength, and crease recovery), functional group content (acid, aldehyde, and ketone), and chain length of the samples were determined. Results indicated that acid degradation was responsible for the major part of the strength loss in the samples treated under aqueous conditions. Under essentially nonaqueous conditions, the majority of the strength loss was due to the cross links. Accessibility of the cross-linked cotton to a swelling agent was also determined and the following results were obtained: control, acid control > Form W > Form D.

13. Cross-Linking of Cotton Cellulose with Ethylene Urea Derivatives Having Varying Hydrogen-Bonding Capabilities Part I: Effects on the Physical Properties and the Hydrogen-Bonded Structure

Cornell Univ. (Agri. Expt. Sta.) (B. Smith)

Cotton print cloth was reacted with 1,3-bis(hydroxymethyl)-2-imidazolidinone(dimethylol ethylene urea) and with several modifications of this compound which had varying hydrogen-bonding capabilities but were still capable of cross-linking the cellulose. Reactions were carried out in two solvent systems, water and dimethylformamide, using $Zn(NO_3)_2 \cdot 6H_2O$ as the catalyst. Add-ons of the cross-linking agents and changes in the physical properties of the treated fabrics were determined. Infrared spectra of the treated fabrics were obtained and infrared bands characteristic of the hydrogen-bonded structure of cellulose were studied and used to qualitatively suggest changes in that structure. It appears that hydrogen bonding of the cellulose with substituents on the resin is not significant in producing changes in the physical properties, including resiliency, of cross-linked cotton. The reactivity of these resins and the type of bond formed with the cellulose system (intra- or inter-molecular) seem to be the major causes of differences in physical properties of the treated fabrics.

14. Crosslinking Cotton Cellulose with Ethyleneurea Derivatives Having Varying Hydrogen-Bonding Capabilities. Accessibility Determinations

Cornell Univ. (Agri. Expt. Sta.) (B. Smith)

In a continuation of previously reported work of the effect on cotton cellulose of ethyleneurea crosslinking agents modified with ring substituents of varying hydrogen-bonding capabilities, accessibilities of the cellulosic hydroxylic protons to exchange with deuterium oxide vapor were determined by means of infrared spectroscopy. In

analyzing these values with respect to previously reported data on physical properties of the treated fabrics, it was found that accessibility to deuterium oxide did not correlate with moisture regain of the resin-treated samples as has been reported for physically modified celluloses. It appears that the different resins did have some effect on the structure of water absorbed by the fiber and also that the solvent affected the manner in which the resins attached themselves to the cellulose and eliminated water from the structure. Values of accessibility were not found to correlate well with crease recovery, although a weak trend was indicated. Accessibility was found to decrease as the infrared band for ring stretching decreased.

15. Fusion Behavior of Linear Polyethylene in Dotriacontane--A DTA Study

NSF

(T. Smith)

An additional crystalline phase has been found to form in linear polyethylene-dotriacontane blends, based on differential thermal analysis (DTA) data. The new phase is formed when blends containing linear polyethylene, at concentrations less than 34 percent, are solidified from the melt under carefully controlled crystallization conditions. The endotherm of the new phase, as measured by the DTA, occurs at 2-5° lower than that of polyethylene. The quantity of the new crystalline phase has been found to be dependent upon polymer molecular weight, blend concentration, solidification rate and heat treatment. Blends having lower molecular weight fractions enhance the formation of the new phase. The relative amounts of the new crystalline phase and the polyethylene crystalline phase vary with the cooling rate of the blend during solidification with the new crystalline phase predominating at slower cooling rates. Heat treatment of the solidified blend results in the merging of the polyethylene and the new crystalline phase endotherms.

16. Acetylene Hydrogenation in a Bubble Column Slurry Reactor

NSF, Res. Board (Univ. of Md.)

(T. Smith)

The hydrogenation of acetylene in a bubble column slurry reactor (BCSR), using Raney nickel catalyst with process water as the inert liquid medium, was studied at several flow rates, temperatures, catalyst loadings, and hydrogen to acetylene feed ratios. The effect of these variables on selectivity, acetylene conversion, and produce distribution was determined. The effect of process time on catalyst activity and selectivity was also investigated. Fractional conversion of acetylene to ethylene and ethane was strongly dependent on process time. This dependence was attributed to polymer formation on the most active sites of the catalyst. After long process time, it is

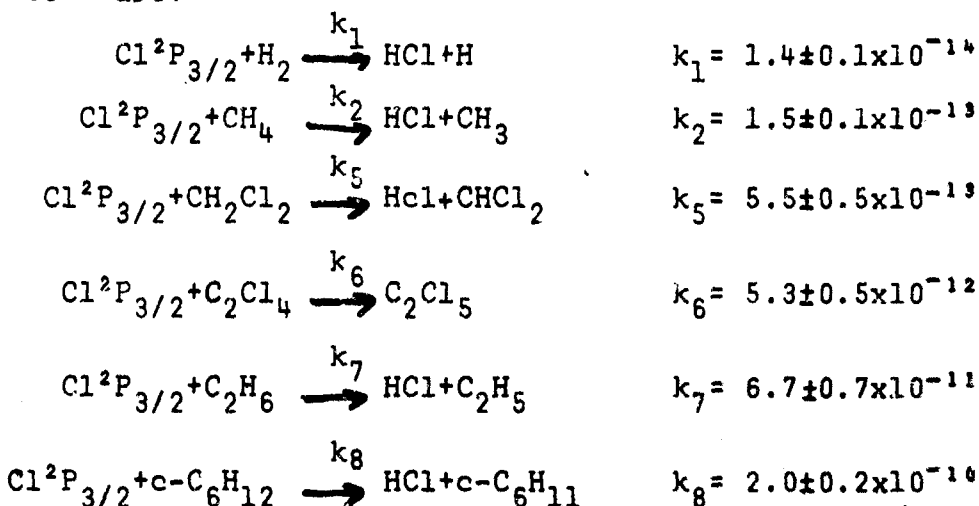
believed that catalyst sites with sufficient activity to permit polymerization are essentially covered with polymer. However, many of the remaining catalyst sites have sufficient activity to allow the reaction, acetylene to ethylene to ethane, to proceed.

17. Reactions of $\text{Cl}^2\text{P}_{3/2}$: Absolute Rate Constants for Reaction with H_2 , CH_4 , C_2H_6 , CH_2Cl_2 , C_2Cl_4 , and $\text{c-C}_6\text{H}_{12}$

NASA

(Davis)

The absolute rate constants have been measured for several gas-phase chlorine atom-molecule reactions at 25°C by resonance fluorescence. These reactions and their corresponding rate constants in units of $\text{cm}^3 \text{mole}^{-1} \text{sec}^{-1}$ are:



The effects of varying the substrate pressure, total pressure, light intensity and chlorine-atom source on the value of the bimolecular rate constants have been investigated for all these reactions. Conditions under which no competing side reaction occurs were established and the reported rate constants were measured under these conditions. For some reactions there is a discrepancy of a factor of two between the rate constants measured in this work and values in the literature; it is suggested that this is due to an error in the previously measured value of $k_{\text{CH}_4}/k_{\text{H}_2}$ upon which the relative measurements in the literature ultimately depend.

18. A Flash Photolysis - Resonance Fluorescence Kinetics Study of Ground State Sulfur Atoms: I. Absolute Rate Parameters for Reaction of $S(^3P)$ with $O_2(^3\Sigma)$.

PRF

(Davis)

The flash photolysis--resonance fluorescence technique has been used to measure the reaction of ground state sulfur atoms with molecular oxygen as a function of both temperature and total pressure. The most suitable source of $S(^3P)$ for this study was found to COS in the presence of CO_2 , as a diluent gas and with the photolysis flash filtered so as to remove all radiation of wavelengths below 1650 \AA . Under these conditions, it was found that over the temperature range of 252-423°K the rate data could be fit to a simple Arrhenius type equation of the form:

$$k_1 = (2.24 \pm .27) \times 10^{-12} \exp \left(\frac{-0.00 \pm 1.10 \text{ kcal/mole}}{RT} \right).$$

Units are $\text{cm}^3 \text{ molec}^{-1} \text{ s}^{-1}$.

The small A factor for this reaction, the lack of any pressure dependence, and the direct observation of the production of $O(^3P)$ with increasing reaction time suggests that the $S(^3P)$ atom attacks the $O_2(^3\Sigma)$ molecule end-on forming SOO which rapidly falls apart to form $SO(^3\Sigma)$ and $O(^3P)$.

19. A Flash Photolysis-Resonance Fluorescence Kinetics Study of Ground State Sulfur Atoms: II. Rate Parameters for Reaction of $S(^3P)$ with C_2H_4

PRF

(Davis)

Absolute rate constants for the reaction of $S(^3P)$ with ethylene were measured over an ethylene concentration range of seven, a total pressure of 5 to 200 torr, and a flash intensity range of ten. At 298°K, the bimolecular rate constant was found to be invariant over this range of variables and had a measured value of $4.69 \times 10^{-12} \text{ cm}^3 \text{ molec}^{-1} \text{ s}^{-1}$. Both COS and CS₂ were used as sulfur atom sources and gave identical results. Over the temperature range of 252 to 423°K, the rate data could be fit to a simple Arrhenius equation of the form:

$$k_1 = (4.624.75) \times 10^{-12} \exp \left(\frac{-1.38 \pm 0.08 \text{ kcal/mole}}{RT} \right).$$

Units are $\text{cm}^3 \text{ molec}^{-1} \text{ s}^{-1}$. Complications arising from the secondary reaction of $S(^3P)$ with the product ethylene episulfide are discussed.

20. Absolute Rate Constants for the Reaction of Atomic Oxygen with 1-Butene over the Temperature Range of 259-493°K

PRF

(Davis)

Several studies have been made of the reaction of atomic oxygen in its ground electronic state with 1-butene. Typically, these investigations have involved the production of atomic oxygen in a mixture of two reactive species with the relative rates of reaction determined by following the rate of production of characteristic reaction products. In only one study, using a discharge flow system, has an absolute rate measurement been made. Because there is a disagreement among the rate measurements, with regard to the reaction's temperature dependence, we have applied the technique of flash photolysis-resonance fluorescence to this system in an effort to better define its kinetic rate parameters.

21. Absolute Rate Constants for the Reaction of Atomic Oxygen with Ethylene over the Temperature Range 232-500°K

PRF, NBS

(Davis)

Rate constants for the reaction of atomic oxygen with ethylene were measured over a temperature range of 232-500°K using the flash photolysis-resonance fluorescence technique. The rate constant at room temperature was also determined using a flash photolysis-kinetic absorption spectroscopy system and a discharge flow system coupled to a mass spectrometer. Within the experimental errors of the three techniques, good agreement was found for the rate constant at 298°K. The bimolecular rate constant was also found invariant to changes in both total pressure and reactant concentration. Over the temperature range of the experiments, the rate data could be fitted by a simple Arrhenius expression of the form:

$$k = 5.42 \pm 0.30 \times 10^{-12} \exp\left(\frac{-114000 \text{ cal/mol}^{-1}}{RT}\right) \text{ cm}^3 \text{ molec}^{-1} \text{ s}^{-1}$$

22. Crystal Surface Morphology Developed During the Sublimation of Oriented Zinc Single Crystals

ARPA

(Armstrong & Bolsaitis)

The surface structure of zinc single crystals subjected to a sublimation treatment has been studied by the techniques of optical metallography, optical goniometry and by Laue x-ray diffraction. Right cylinders with an <0001> axis were enclosed, with titanium getterer material, in vycor tubes evacuated to 10^{-4} mm Hg and heated to temperatures in the vicinity of 370°C for periods of

100 to 200 hours. A thermal gradient existed in the evacuated chamber such that zinc was transported from one end of the tube to the other end. The sublimation process exposed macroscopically visible crystallographic planes in local regions of the crystals. The three-dimensional structure of the facet morphology has been determined. The exposed planes are of the type {1010}, {4041}, {3031}, {3032}, {1011}, {4045}, {2023}, and {101 10}. The {0001} surfaces were relatively unaffected by the sublimation process. The facet structures appear to be related to some extent to the dislocation substructure and also to the Gibbs-Wulff surface energy construction for zinc.

23. The Crystal Structure of Methylene Blue

NASA, WRAE

(Stewart)

The crystal structure of Methylene Blue hydrochloride pentahydrate reveals sheets of Methylene Blue molecules associated with chloride ions on the terminal nitrogens within a clathrate-like network of water molecules perpendicular to the planes formed by the phenazathionium units.

24. The Molecular Structure of 1,1-Dimethyl-3-Phenylpyrazolium-5-Oxide

NASA

(Stewart)

The molecular structure of 1,1-dimethyl-3-phenylpyrazolium-5-oxide has been determined by a single crystal x-ray diffraction study. The crystals are monoclinic, space group P2₁/a, with unit cell dimensions a=12.633(5)Å, b=6.644(1)Å, c=12.486(5)Å, β=99.17(2)°. The final R value was 0.049 for 2930 reflections. The bond lengths and angles suggest that a significant contribution to the structure is made by a resonance form in which one of the ring bonds does not exist. No close intermolecular approaches were found.

25. Scanning Electron Microscope Study of Polyethylene Spherulites

ARPA

(Jackson & Marcinkowski)

A detailed scanning electron microscope study has been made of spherulites of melt-crystallized polyethylene. A new model is proposed for the twisted lamellae which cause the concentric bands seen in polyethylene spherulites in the polarizing microscope. Successive bands correspond to alternate left and right handed twists of the lamellae. In contrast to the more generally accepted helical twist model, this new model satisfactorily explains the space filling in spherulites, and it is compatible with SEM observations of unetched, ion etched,

and nitric acid etched polyethylene samples. In the unetched samples the spherulite topography develops as a function of time under the electron beam of the SEM and is believed to be due to surface heating of the sample.

26. Mean-Square Atomic Displacements in HgTe and their Temperature Dependence

(Bolsaitis)

The mean-square atomic displacements and associated Debye temperature of HgTe have been determined from single crystal x-ray scattering measurements at 32°, 90°, and 296°K. The mean-square displacements of Hg and Te are observed to increase from $0.0064 \pm 0.0001 \text{ \AA}^{-2}$ and $0.0055 \pm 0.0001 \text{ \AA}^{-2}$ to $0.029^{+0.011}_{-0.003} \text{ \AA}^{-2}$ and $0.0209^{+0.0046}_{-0.0021} \text{ \AA}^{-2}$, respectively, while the corresponding Debye temperature increases from $73 \pm 1 \text{ K}$ to 101^{+6}_{-13} K , over this temperature range. Comparison is made with other similar measurements and with recent theoretical calculations for HgTe; differences are noted and discussed. The results reported here tend to substantiate the experimental work upon which a recently reported failure of the Brooks-Yu theory for HgTe is based.

H. OPTICAL AND SPECTROSCOPIC PROPERTIES OF MATERIALS

1. Optical Absorption of Sodium ARPA, ONR, AFOSR

(Bardasis)

The imaginary part of the transverse dielectric tensor has been calculated for sodium using a two-band model and including both phonons and the interactions between conduction electrons in the random-phase approximation. It is found that the resulting expression reduced to the Hopfield dielectric constant for the case of an electron gas in a perturbing crystal potential. Reasonable agreements with N.V. Smith's data has been found in the range of photon energies 0.5-3.0 eV. However, at higher energies the agreement is not as good, since many-body effects become more important in this region.

2. Single-Crystal Infrared and Raman Spectra of Cyanuric Chloride

ARPA, Dept. of Defense, ARO, PHR

(Lippincott)

The single-crystal infrared and Raman spectra of cyanuric chloride, 1,3,5-trichlorotriazine, were measured at 298 and 77°K. A complete assignment for the intramolecular fundamentals was made, including a study of a modified valence force field. Intensity predictions from the oriented gas model qualitatively agreed with the experimental results for the intensity of the free molecule Raman-active bands. Spectral measurements in the low-frequency region resulted in the assignment of several bands to the optically active lattice modes of cyanuric chloride.

3. Inelastic Neutron Scattering from b.c.c. ^4He AEC

(Minkiewicz)

Inelastic neutron scattering experiments have been carried out on large single crystals of the quantum solid, ^4He . The crystals were oriented in the [011] zone and had volumes larger than 5cm^3 . Both transverse and longitudinal excitations were studied with propagation vectors along the [100], [111], and [011] principal symmetry directions. Dispersion relations along these three symmetry directions are presented and discussed within the context of the results of recent theories for this highly anharmonic solid. The data, which presents clear evidence for strong phonon relaxation, is also compared with theoretical line width estimates. The elastic constants calculated from these data are $c_{11}/\rho = 1.77 \pm 0.32$, $c_{33}/\rho = 1.58 \pm 0.35$, and $c_{44}/\rho = 1.07 \pm 0.10$ in units of $10^5 \text{ m}^2/\text{sec}^2$, in good agreement with the results obtained from ultrasonic and thermodynamic measurements. When the amplitude of the scattering vector $|Q|$ approaches

1.6a, some extra intensity is observed near an energy of 1.4meV. Evidence that this intensity is indeed real and anomalous, some four times as much as expected from single phonon scattering, is presented. The physical origin of this extra scattering is not presently known.

4. Vibronic Effects in Hydrogen Bonding
NSF

(Lippincott)

Vibronic states of model hydrogen (H) bonded systems X-H...X are computed using a numerical solution to the Schrodinger equation. From the calculated energy eigenvalues, model properties are derived and compared with those experimentally observed in H bonded systems. Numerous trends of the strong and weak H bonds are duplicated in the model systems, and some of the anomalous variances of structural and spectroscopic properties with isotropic substitution (D for H) are calculated, also.

The importance of the H atom vibrational contribution to the energy of the H bond is of particular interest in this study. The Born-Oppenheimer Approximation is extended beyond solely electronic energy considerations to include the light atom (H or D) kinetic energy terms. As the zero-point energy of a particle in a box decreases when the size of the box is enlarged, the energy of a X-H vibrator decreases when juxtaposed with an appropriate H acceptor to form the X-H...X bond. The relative importance of this vibrational energy bonding term is found to be of the same order of magnitude as the energy derived from purely electronic interactions of the H bond. $\Delta E_{(vib.)}/\Delta E_{(\text{Total})} = 23-33\%$. Although the relative importance of the net vibration energy to the H bond may vary beyond the limits found in this study, the effect is thought to be general. A name might be suggested for this part of the bond energy, the "vbond" so that no confusion need arise in referring to this effect.

$$\text{H Bond} = \text{Electronic Interaction} + v \text{ Bond}$$

5. A Linear Technique for the Measurement of Ultrashort Optical Pulse Widths
ARO, NRL

(Alley)

A technique for the measurement of the widths of ultrashort optical pulses which does not involve any nonlinear processes is described. Also it is shown that for a pulse with a small rise time this technique can be used to produce a pulse whose width is approximately equal to the rise time of the original pulse.

6. Far-Field Diffraction Pattern for Corner Reflectors
with Complex Reflection Coefficients
NASA, CSC (Alley)

The far-field diffraction pattern of a geometrically perfect corner reflector is examined analytically for normal incident monochromatic light. The states of polarization and the complex amplitudes of the emerging light are expressed, by use of transformation matrices, in terms of those of the original incident light for each sextant of the face in a single coordinate system. The analytic expression of the total diffraction pattern is obtained for a circular face. This expression consists of three component functions in addition to the basic Airy function. The coefficient of each function is expressed in terms of complex coefficients of reflectance of the reflecting surface. Some numerical results for different reflecting surfaces, including total internal reflection, are presented. The iso-irradiance contours of the diffraction pattern evaluated from the analytical expressions for an uncoated solid corner reflector are also presented, along with photographs of the pattern.

7. GaAs-Laser-Induced Population Inversion in the Ground-State Hyperfine Levels of Cs¹³³
NASA, ARPA, ARO (Alley)

This paper describes the achievement of population inversion among the hyperfine levels in the ground state of Cs¹³³ by optically pumping these atoms with radiation from a GaAs diode laser. The laser output was used to monitor the populations in the two ground-state hyperfine levels as well as to perform the hyperfine pumping.

By varying the injection current, a GaAs laser operated CW at about 77°K, was used to scan the 8521-Å line of Cs¹³³. The intensity of the resonance scattering from cesium vapor served as an indicator of the populations of the two levels involved. Experiments were performed both with neon-filled and with para-flint-coated cells containing the cesium vapor.

It was discovered that the diode laser could easily be tuned by manually adjusting the injection current to match either of the hyperfine components of the D₂ optical transition.

Possible future applications, including a restudy of the light shifts, the construction of a cesium maser, and the physics of optical pumping with coherent light are discussed.

8. Long Wavelength Phonon Spectra of $\text{Na}_2\text{ZnCl}_4 \cdot 3\text{H}_2\text{O}$ and
 $\text{Na}_2\text{ZnCl}_4 \cdot 3\text{D}_2\text{O}$
ARPA, AROD

(Lippincott & Khanna)

The transverse-longitudinal (T-L) splittings of the A_1 and E phonons of $\text{Na}_2\text{ZnCl}_4 \cdot 3\text{H}_2\text{O}$ and $\text{Na}_2\text{AnCl}_4 \cdot 3\text{D}_2\text{O}$ have been observed by choosing the proper scattering geometries in Raman experiments. A number of phonons, eg. the A_1 and E components of v_3 (H_2O), the E component of $v_3(\text{ZnCl}_4^=)$, and an E component of a H_2O torsional mode, had T-L splittings greater than 10 cm^{-1} . Comparison of the T-L splittings and the correlation field splittings of the internal modes of H_2O in this crystal reveals that H_2O modes having large T-L splittings generally exhibit small correlation field splittings. The $\text{H}\cdots\text{H}$ non-bonded interactions may be important in explaining the observed correlation splittings.

9. Signal-to-Noise Ratio in Atomic Fluorescence Flame Spectrometry and Condensed-phase Inorganic Fluorimetry
(O'Haver)

In a previous article the authors have given a summary of the equations for the luminescence radiance in atomic fluorescence flame spectrometry and in condensed-phase inorganic fluorimetry. In this installment, we present expressions relating the luminescence radiance to the photodetector signal. An explanation of the basic aspects of noise, bandwidth, noise sources, and the signal-to-noise ratio is also given.

10. Long Wave-Length Optical Phonons of Sodium Chlorate at 77°K
ARPA

(Khanna)

A detailed examination of the Raman spectra of NaClO_3 at liquid N_2 temperature has revealed some results different from those previously reported.

11. Spectrum and Structure of the He_2 Molecule VI. Characterization of the States Associated with the UAO's $3\text{p}\pi$ and 2s
NASA, NSF, Univ. of Md.
(Ginter)

The He_2 band systems $3\text{p}\pi ^1\text{A}^1\text{IIg}+2\text{s}^1, ^3\Sigma_u^+$ are described in detail. Characterization of the 2s , $a^3\Sigma_u^+$ and $A^1\Sigma_u^+$ states and the $3\text{p}\pi$, $e^3\text{II}_g$ states has been extended through

$v \approx 5$. The effects of A-doubling are considered, and various molecular constants (cm^{-1}) are reported.

12. Electronic Spectra and Structure of the Hydrogen Halides. States Associated with the $(\sigma^2\pi^3)c\pi$ and $(\sigma^2\pi^3)c\sigma$ Configurations of HCl and DCl.

E.O.Hulbert Ctr. for Space Res.

(Ginter)

High resolution absorption spectra of HCl and DCl have been analyzed in the region from ~ 1200 to $\sim 1240\text{\AA}$. Almost all of the observed band structure can be associated with the $d^1\Pi_j$, $D^1\Pi$, and $f^3\Delta_j + X^1\Sigma^+$ transitions, where the upper states are correlated with the $(\sigma^2\pi^3)c\sigma$ and $(\sigma^2\pi^3)c\pi$ configurations. In HCl, the $c\sigma$ and $c\pi$ orbitals should correspond most nearly to $4p\sigma$ and $4p\pi$, respectively. This wavelength region also contains a portion of a long progression of bands which are assigned to the $V^1\Sigma^+ + X^1\Sigma^+$ transition. It appears that the 0^+ states from the $(\sigma^2\pi^3)c\pi$ configuration interact strongly with the $V^1\Sigma^+$ state.

13. Electronic Spectra and Structure of the Hydrogen Halides. States Associated with the $(\sigma^2\pi^3)c\pi$ and $(\sigma^2\pi^3)c\sigma$ Configurations of HBr and DBr

NRL

(Ginter)

The high resolution absorption spectra of HBr and DBr have been reinvestigated in the spectral region below 79500cm^{-1} . Except for bands assigned to the $V^1\Sigma^+ + X^1\Sigma^+$ transition and those previously identified as the $b^3\Pi + X^1\Sigma^+$ and $C^1\Pi + X^1\Sigma^+$ transitions, all bands which have been observed may be assigned to transitions in which the upper states originate from either the $(\sigma^1\pi^3)c\sigma$ or $(\sigma^2\pi^3)c\pi$ excited configurations. In HBr $c\sigma$ and $c\pi$ should correspond most nearly to $(5p\sigma)$ and $(5p\pi)$, respectively, while the electronic states associated with these configurations closely approach pure Ω, ω coupling. Rotational and vibrational data are presented for all observed transitions to the $d^1\Pi_j$, $D^1\Pi$, $f^3\Delta_j$, $F^3\Delta$, $E0^+$, and $g0^+$ states.

SECTION III
FACULTY PARTICIPATING IN MATERIALS RESEARCH

Name	Title	Department
C. O. Alley	Associate Professor	Physics
J. R. Anderson	Associate Professor	Physics
R. W. Armstrong	Professor	Mechanical Engineering
R. J. Arsenault	Associate Professor	Chemical Engineering
***R. J. Asimow	Associate Professor	Mechanical Engineering
W. J. Bailey	Professor	Chemistry
A. Bardasis	Associate Professor	Physics
J. M. Bellama	Assistant Professor	Chemistry
S. M. Bhagat	Associate Professor	Physics
P. P. Bolsaitis	Assistant Professor	Chemical Engineering
**A. Charlesby	Professor	Chemical Engineering
D. D. Davis	Assistant Professor	Chemistry
H. D. Drew	Assistant Professor	Physics
W. Elsasser	Professor	Fluid Dynamics
D. S. Falk	Associate Professor	Physics
***R. A. Ferzell	Professor	Physics
*M. Ginter	Associate Professor	Molecular Physics
A. J. Glick	Associate Professor	Physics
R. Glosser	Assistant Professor	Physics
R. E. Glover, III	Professor	Physics
*G. Gordon	Assistant Professor	Chemistry
S. O. Grim	Professor	Chemistry
G. Helz	Assistant Professor	Chemistry

Name	Title	Department
U. Hochuli	Associate Professor	Electrical Engineering
J. F. Jackson	Assistant Professor	Chemistry
R. K. Khanna	Assistant Professor	Chemistry
H. Kim	Associate Professor	Electrical Engineering
*J. F. Koch	Associate Professor	Chemistry
V. Korenman	Assistant Professor	Physics
L. Krisher	Associate Professor	Mol. Physics
C. H. Lee	Assistant Professor	Electrical Engineering
*H. C. Lin	Professor	Electrical Engineering
*E. R. Lippincott	Professor	Chemistry
C. Maltz	Assistant Professor	Mol. Physics
*M. Marcinkowski	Professor	Mechanical Engineering
P. H. Mazzocchi	Associate Professor	Chemistry
G. Miller	Associate Professor	Chemistry
T. O'Haver	Assistant Professor	Chemistry
R. Prange	Professor	Physics
J. V. Sengers	Associate Professor	Mol. Physics
*J. Silverman	Professor	Chemical Engineering
L. Skolnick	Professor	Chemical Engineering
B. F. Smith	Professor	Textiles & Consumer Econ.
T. G. Smith	Professor	Chemical Engineering
S. E. Sommer	Assistant Professor	Chemistry
I. L. Spain	Associate Professor	Chemical Engineering
J. M. Stewart	Professor	Chemistry
W. H. Zoller	Assistant Professor	Chemistry

*CMR Advisory Committee
 **Visiting Professor
 ***Sabatical

SECTION IV
RESEARCH ASSOCIATES

<u>Name</u>	<u>Department</u>
G. Anderson	Chemistry
E. Barry	Chemistry
P. K. Basu	Chemical Engineering
E. Baumgartner	Chemistry
G. Cessac	Chemistry
R. F. Chang	Physics
R. Doezena	Physics
J. R. Dorfman	Fluid Dynamics
H. Drew	Physics
G. Kruger	Chemistry
A. MacCragh	Chemistry
A. Mears	Physics
R. Patel	Chemistry
E. Pink	Chemical Engineering
M. Schneider	Chemistry
D. Stroman	Chemistry
M. Wihl	Physics
C. Ch. Wu	Mechanical Engineering
H. Preston	Chemistry
R. G. Churchill	Chemistry
R. J. Fernandez-Prini	Chemistry
J. O. Henningsen	Physics

Name

E.S.P. Das
K. Sadananda
Y. Huang

Department

Mechanical Engineering
Mechanical Engineering
Chemical Engineering

SECTION V

GRADUATE STUDENTS PARTICIPATING IN MATERIALS RESEARCH PROGRAMS

J. Alcantara	Physics
G. Arnstein	Mechanical Engineering
S. Babu	Physics
J. Benson	Chemistry
V. Bharthumnavin	Electrical Engineering
M. Bowen	Chemistry
W. Briggs	Chemistry
D. Campbell	Chemistry
H. Chang	Chemical Engineering
R. Chao	Chemistry
C. Clark	Chemical Engineering
C. Cody	Chemistry
M. Maaghoul	Chemical Engineering
R. Davis	Physics
J. Davison	Chemistry
J. DelGaudio	Chemistry
F. Feizollaki	Chemical Engineering
S. Fong	Mechanical Engineering
L. Gerchman	Chemistry
E. Gladney	Chemistry
J. Green	Chemical Engineering
E. Grim	Textiles & Consumer Econ.
J. Gryzbowski	Chemistry
R. Gsell	Chemistry
I. Halchak	Chemistry
G. Hammer	Electrical Engineering
L. Harton	Chemistry
A. Hart	Chemistry
T. Hsu	Chemistry
Y. Hsueh	Electrical Engineering
J. Hudak	Physics
B. Huie	Chemistry
K. Ishizaki	Chemical Engineering
C. Jameson	Chemistry
S. Jayaraman	Electrical Engineering
A. Kangar	Physics
B. Klemm	Chemistry
K. Kuo	Chemical Engineering
P. Lasken	Physics
J. Lee	Physics

A. Liu	Physics
K. Liu	Chemical Engineering
R. Lustig	Chemistry
N. Madhava	Mechanical Engineering
B. Majane	Chemistry
L. Matienzo	
M. Moradi	Chemistry
J. Mitchell	Chemistry
J. Morrison	Chemistry
J. Oravek	Chemistry
S. Pal	Physics
W. Payne	Chemistry
A. Pyzik	Chemistry
A. Rowek	Chemical Engineering
M. Shimiju	Chemical Engineering
P. Samantary	Mechanical Engineering
S. Segal	Chemical Engineering
D. Shah	Chemistry
K. Sibbald	Physics
B. Slaten	Textiles & Consumer Econ.
U. Strom	Physics
W. Tseng	Mechanical Engineering
W. Tung	Chemical Engineering
J. vanDeeren	Physics
W. Wong	Chemistry
Y. Wu	Chemistry

SECTION VI
PUBLICATIONS

1. C. O. Alley, G. Singh and F. Dilavore, GaAs Laser Induced Population Inversion in the Ground State Hyperfine Levels of CS⁺, Journal of Quantum Electronics 7, May 1971.
2. C. O. Alley, R. F. Chang, D. G. Currie and M. F. Pittmen, The Far Field Diffraction Pattern for Corner Reflectors with Complex Reflection Coefficients, Journal of the Optical Society of America 61, 431 (1971).
3. C. O. Alley and R. L. Smith, A Linear Technique for the Measurement of Ultrashort Optical Pulse Widths, Optics Communication 1, 262 (1970).
4. J. R. Anderson, J. E. Schirber and D. R. Stone, Pressure Studies of the Fermi Surface of Thallium, Grenoble High Pressure Conf. Proceedings, No. 188 (1970).
5. J. R. Anderson, F. L. Cheng and S. M. Bhagat, Ferromagnetic Resonance in Single Crystal Nickel Disks: Angular Dependence of Resonance Field and Linewidth, Phys. Stat. Sol. (b) 45, 357 (1971).
6. J. R. Anderson and D. C. Hines, The de Haas-van Alphen Effect in Dilute Alloys of Bismuth in Lead, Phys. Rev., 2B, 4752 (1970).
7. J. R. Anderson, J. J. Hudak and D. R. Stone, dHvA Oscillations in Cobalt Spheres, Proceedings of the 1971 Conference on Magnetism and Magnetic Materials, AIP Conference Proceedings Series.
8. R. W. Armstrong, C. T. Liu and J. Garland, Friction 1 Stress and the Yield and Flow Behavior of Iron Polycrystals and Carbon Steels, J. Iron Steel Inst. 209, 142 (1971).
9. R. W. Armstrong and E. Pink, Total Material Variables Influencing a Ductile-Brittle Transition Temperature for Molybdenum, Z. F. Metallkunde 6, 147, (1971).
10. R. W. Armstrong, B. Arkayin and G. Haddad, Fracture of Bone Material in Compression at Temperatures in the Interval -200° to +200°C, Nature 232, 576 (1971).
11. R. W. Armstrong, A. C. Paghuram and R. E. Reed, Solute-Subgrain Boundary Interaction in Niobium, Mat. Sci. and Engineering 8, 299 (1971).
12. R. W. Armstrong, C. Qm. Wu and C. H. Lee, Berg-Barrett X-ray Observation of Annealing and Laser Induced Damage in Zinc, University of Md. Engr. Mat. Group Rept. LXI, J. Appl. Phys. (December, 1971), in print.
- 12a R. W. Armstrong, P. P. Bolsaitis and G. M. Arnstein, Crystal Surface Morphology developed during the Sublimation of Oriented Zinc Single Crystals, (accepted for publication in Acta. Cryst. (1971)).
13. R. J. Arsenault and E. Pink, The Effect of Neutron Irradiation and Oxygen Interstitials on the Dislocation Dynamics in Vanadium, Mat. Sci. Eng. 8, 141 (1971).

14. R. J. Arsenault and D. F. Hasson, The Relaxation Strength A per Atomic Percent Solute - a/o for Oxygen in Vanadium, Scripta Met. 5, 75 (1971).
15. R. J. Arsenault, The Entropy of Thermally Activated Plastic Deformation, Met. Trans. 2, 1472 (1971).
16. R. J. Arsenault and D. F. Hasson, Unusual Fracture Features of Oxidized Vanadium + 1.31 at % Titanium Alloy, Mat. Sci. Eng. 7, 215 (1971).
17. R. J. Arsenault and H. A. Beale, An Investigation of Methods of Preparing High Purity Vanadium, Fourth Int'l Conference on Electron and Ion Beam Science and Technology, Ed. R. Bakish, Elec. Soc., N. W., 1971, p. 421.
18. R. M. Asimow and S. P. Makhijani, Deformation Induced Resistivity Changes in Single Crystal Ag-Au Alloys, Scripta Met. 4, 63 (1970).
19. R. M. Asimow and V. K. Iyer, Computer Simulation of Short Range Ordering, submitted to Phys. Rev.
20. R. M. Asimow, D. Rosenthal and Van Nostrand, Introduction to Properties of Materials, Sec. Ed., In press (book).
21. R. M. Asimow and P. Samal, Critical Resolved Shearing Stress of a Silver 2.9% Indium Alloy a Function of Growth Rate, Mat. Sci. Eng. 18, (1971).
22. W. J. Bailey and L. J. Baccei, Mechanisms of the Thermal Degradation of Polyethylene, Am. Chem. Soc., Div. Polymer Chem., Preprints 12, No. 2, 313 (1971).
23. W. J. Bailey and C. F. Beam, A Convenient Preparation of Cyclohexane-1, 4-dicarboxaldehyde and Cyclohexane-1, 1,4, 4-tetraanol, J. Chem. Soc. c, 2730 (1971).
24. W. J. Bailey and L. J. Baccei, Mechanisms of the Thermal Degradation of the Regular Alternating Copolymer of Ethylene and Deuteroethylene, XXIII International Congress of Pure and Applied Chemistry, Macromolecular Preprint, Vol. II, Boston, Mass., July 25-30, 1971, p. 776.
25. W. J. Bailey, Diels-Alder Polymerization, in Step-Growth Polymerization, D. H. Solomon, ed., Marcel Dekker, Inc., New York, N. Y., 1971.
26. W. J. Bailey, C. F. Beam, Jr. and I. Haddad, New Spiro Polymers Containing Five-, Six-, Seven-, and Eight-Membered Cyclic Metals, Am. Chem. Soc., Div. Polymer Chem., Preprints, 12 169 (1971).
27. A. Bardasis and A. S. Karakashian, Phonon Contribution to the Optical Properties of Sodium, Phys. Letters A139 (1970).
28. A. Bardasis and A. S. Karakashian, Optical Absorption of Sodium, Phys. Rev. B 4, 404 (1971).
29. J. M. Bellama, L. C. Krisher and R. A. Gsell, The Microwave Spectra of Chlorostannane, J. Chem. Phys. 54, 2287 (1971).
30. J. M. Bellama and C. J. McCormick, Synthesis and Properties of Isomeric Monohalogeno Derivatives of Methylgermane, Inorg. Nucl. Chem. Lett., 533 (1971).

31. J. M. Bellama, J. J. Ritter and T. D. Coyle, Reactions of Diboron Tetrahalides with Haloolefins. Formation of poly(dihaloryl)ethanes, J. Organometal. Chem. 29, 175 (1971).
32. S. M. Bhagat and R. A. Lasken, Depression of T_A by a Heat Current, to be published in Phys. Rev. (1971).
33. S. M. Bhagat and R. S. Davis, Influence of a D.C. Heat Flux on the Velocity of Second Sound Near T_A , to be published in Journal of Low Temperature Physics (1972).
34. S. M. Bhagat and R. A. Lasken, HeII-HeI Transition in a Heat Current: Model Calculations, Phys. Rev. A, 2, 264 (1971).
35. S. M. Bhagat and R. S. Davis, The Velocity of Second Sound in a Heat Current, Phys. Lett. 34A, 233 (1971).
36. S. M. Bhagat, V. Chopra and R. K. Ray, Low Temperature Resistivity of Bi and its Alloys, Phys. Stat. Sol. 4, 205 (1971).
37. S. M. Bhagat, J. R. Anderson and F. L. Cheng, Ferromagnetic Resonance in Single Crystal Nickel Disks: Angular Dependence of Resonance Field and Linewidth, Phys. Stat. Sol. (b) 45, 357 (1971).
38. P. P. Bolsaitis, G. M. Arnshtain and R. W. Armstrong, Crystal Surface Morphology developed during the Sublimation of Oriented Zinc Single Crystals, (accepted for publication in Acta. Cryst. (1971)).
39. P. P. Bolsaitis and K. Hsueh, An Equation of State of the Noble Metals, (to be published in T. of Phys. and Chem. of Solids (1971)).
40. P. P. Bolsaitis, E. F. Skelton, P. L. Radoff and T. Verbalis, Mean-Square Atomic Displacements on Hg-Te and their Temperature Dependencies, (to be published in Phys. Rev. (1971)).
- * See #150 for D. D. Davis publications.
41. H. D. Drew and U. Strom, Electron Relaxation Rates in Bismuth at Microwave and Far Infrared Frequencies, Phys. Rev. Letters 25, 1755 (1970).
42. H. D. Drew, U. Strom and J. F. Koch, Quantum Aspects of the Azbel'-Kaner Resonance in Bismuth, Bull. Am. Phys. Soc. 16, 358 (1971) and Phys. Rev. Letters 26, 1110 (1971).
43. H. D. Drew, Retardation Effects in Azbel'-Kaner Cyclotron Resonance, to be published Phys. Rev..
44. H. D. Drew, R. E. Doezena and J. Restorff, Optical Absorption of Cu-Ni Alloys, Bull. Am. Phys. Soc. 16, 845 (1971).
45. D. S. Falk, Helicons, Doppler-Shifted Cyclotron Resonance, and Gantmakher-Kaner Oscillations. II. p-Fold Azimuthal Symmetry, Phys. Rev. B 3, 1973 (1971).
46. D. S. Falk and J. O. Henningsen, Time-of-Flight Effects in Microwave Transmission Through a Thin Metal Slab, Phys. Rev. Letters 26, 1174 (1971).

47. R. A. Ferrell, Decoupled-Mode Dynamical Scaling Theory of the Ferromagnetic Phase Transition, Proceedings of the Int'l Conference of Magnetism, Grenoble, J. of Phys. 32, January (1971).
48. R. A. Ferrell, Decoupled-Mode Dynamical Scaling Theory of Phase Transitions, Proceedings of Conference on Dynamics of Critical Phenomena, Fordham Univ., New York, June 1970, Editor J. Budnick.
49. R. A. Ferrell, Decoupled-Mode Dynamical Scaling Theory of the Binary Liquid Phase Transition, Phys. Rev. Lett. 24, 1169 (1970).
50. M. L. Ginter and C. M. Brown, The Spectrum and Structure of the He₂ Molecule. VI. Characterization of the States Associated with the UAO'S 3p₁ and 2s, J. Mol. Spectry. 38, 000 (1971).
51. M. L. Ginter and S. G. Tilford, Electronic Spectra and Structure of the Hydrogen Halides. States Associated with the (σ π)cm and (σ π)c Configurations of HBr and DBr, J. Mol. Spectry. 37, 159 (1971).
52. M. L. Ginter and S. G. Tilford, Electronic Spectra and Structure of the Hydrogen Halides. States Associated with the (σ π)cm and (σ π)c Configurations of HCl and DCl, J. Mol. Spectry. 38, 000 (1971).
53. M. L. Ginter and C. M. Brown, Dissociation Energies of X²Σ⁺ (He₂⁺) and A¹Σ⁺ (He₂), J. Chem. Phys. 56, 0000 (1972).
54. M. L. Ginter, S. G. Tilford R. Howard, Fluorescence of Carbon Monoxide Excited by the 1306 Å Oxygen Resonance Line, J. Chem. Phys. 56, 000 (1972).
55. A. J. Glick and W. F. Long, An Asymptotic Form of the Dissipating Part of the Complex Dielectric Constant for a Degenerate Electron Gas, Bull. Am. Phys. Soc. Ser. II, 16, 543 (1971).
56. A. J. Glick and W. F. Long, High Frequency Damping in a Degenerate Electron Gas, Phys. Rev. B 4, 3455 (1971).
57. R. Glosser and W. C. Walker, Electroreflectance Observation of Localized and Itinerant Electron States in NiO, Solid State Comm. 9, 1399 (1971).
58. R. Glosser, J. E. Fischer and B. O. Seraphin, Interconduction Band Transitions in the Electroreflectance Spectrum of InSb, Phys. Rev. B 1, 1607 (1970).
59. R. E. Glover, III, Superconductivity above the Transition Temperature, being published in Progress in Low Temperature Physics.
60. R. E. Glover, III, Stefan Moser and Friedhold Baumann, Superconducting Beryllium Films, Being published in Phys. Rev. (1970).
61. R. E. Glover, III and W. Falsch, Effect of Surface Charge on the Superconducting Transition Temperature and Normal-State Conductivity of Disordered Metal Films, to be published in the J. of Vacuum Science and Technology.
62. S. O. Grim and R. A. Ference, Tertiary Phosphine Complexes of Rhodium(III) and Rhodium(I), Inorganica Chimica Acta 4, 277-282 (1970).

63. S. O. Grim and R. L. Keiter, A Phosphorous-31 Magnetic Resonance Study of Tertiary Phosphine Palladium (II) Compounds, Inorganica Chimica Acta 4, 56-60 (1970).
64. S. O. Grim, A. W. Yankowsky and W. L. Briggs, Preparation of 2-Diphenylphosphineethylphosphinites, Chemistry and Industry (London), 375 (1971).
65. S. O. Grim, E. F. Davidoff and T. J. Marks, Preparation and 31p Chemical Shifts of Some Quaternary Phosphonium Salts, Z. Naturforschung 26b, 184-190 (1971).
66. S. O. Grim, H. J. Plastas, C. L. Huheey and J. E. Huheey, Bond Angles, Hybridization, and Phosphorus-Metal Bonding, Phosphorus 1, 61-65 (1971).
67. U. E. Hochuli, Technical Report #1 for NASA Grant NGR-21-002-216, GaAs CO₂ Laser Window Sealing Technique, Aug. 1970.
68. U. E. Hochuli, Technical Report #2 for NASA Grant NGR 21-002-216, CO₂ Laser Life Study, Jan. 1971.
69. U. E. Hochuli, Relative Frequency Stability of Stable He-Ne Gas Laser Structures, Journal of Quantum Electronics, in press.
70. J. F. Jackson, T. S. Hsu and J. W. Brasch, A Newly Discovered Morphological Feature of Crystalline Polyethylene, Polymer Preprints 12 (2), 537 (1971).
71. J. F. Jackson, Melting Behavior of Radiation Crosslinked Crystals of Polyethylene, XXIII IUPAC Macromolecular Preprints, Vol. II, 845 (1971).
72. J. F. Jackson, J. Breedon, M. J. Marcinkowski and M. E. Taylor, Jr., Scanning Electron Microscope Study of Polyethylene Spherulite, J. Polymer Sci., A-2, in press.
73. J. F. Jackson, T. S. Hsu and J. W. Brasch, Direct Microscopic Observation of the Crystallization Process of Polyethylene at High Pressure: Acicular or Bladed Crystals, J. Polymer Sci., B, in press.
74. J. F. Jackson, P. J. Miller and R. S. Porter, IR Dichroism Study of Polyethylene Crystallized Under the Orientation and Pressure Effects of a Pressure Viscometer, to be submitted to J. Polymer Sci.
75. R. K. Khanna and P. J. Miller, Long Wavelength Phonon Spectra of Sodium Chlorate, Spectrochim. Acta 27A, 927 (1971).
76. R. K. Khanna, G. Cessac, E. R. Lippincott and A. R. Bandy, Long Wavelength Phonon Spectra of Na₂AnCl₄·3H₂O and Na₂AnCl₄·3H₂O, Spectrochim. Acta, in press.
77. J. F. Koch and R. E. Doezeema, Quantum Aspects of the Azbel'-Kaner Resonance in Bismuth, Phys. Rev. Lett. 25, 1110 (1971).
78. J. F. Koch, A. Kamgar and J. O. Henningsen, An Experimental Study of Retardation Effects in Cyclotron Resonance, to be published in Phys. Rev.
79. J. F. Koch, K. E. Sibbald and A. L. Mears, rf Surface Impedance in the Presence of Magnetic-Field-Induced Surface States, Phys. Rev. Lett. 27, 14 (1971).

80. J. F. Koch, H. D. Drew and U. Strom, Quantum Aspects of the Azbel-Kaner Resonance in Bismuth, Bull. Am. Phys. Soc. 16, 358 (1971) and Phys. Rev. Letters 26, 1110 (1971).
81. V. Korenman, Photon Counting, Correlation Functions, and the Critical Region, Phys. Rev. A 2, 449 (1970).
82. V. Korenman and J. Keller, Regularization of the Maki Conductivity by Fluctuations, Phys. Rev. Letters 27, (1971).
83. V. Korenman and R. E. Prange, Line Width of Ferromagnetic Resonance in Metals, Journal of Magnetic Resonance (to be published).
84. C. H. Lee and R. C. Eckardt, Measurement of Ultrashort Light Pulses Using Optical Third Harmonic Generation, Bull. of Amer. Phys. Soc., Vol. 15, No. 1, 88 paper GE-5 (1970).
85. C. H. Lee and S. Hayaraman, Observation of Two Photon Conductivity in GaAs by a Giant Pulse Nd: glass Laser, Bull. of Am. Phys. Soc., Vol. 15, No. 4, p. 653, paper K1 12, April 1971.
86. C. H. Lee, C. On. Wu and R. W. Armstrong, Berg-Barrett X-ray Observation of Annealing and Laser Induced Damage in Zinc, J. of Appl. Physics (to be published, December 1971).
87. C. H. Lee, R. C. Eckardt and J. Bradford, Investigation of Temporal and Spectral Development of a Nd: glass Laser with a Ring Cavity, Appl. Phys. Lett., (to be published in No. 10, Vol 19, November 1971).
88. H. C. Lin, Comparison of Input Offset Voltage of Differential Amplifiers Using Bipolar Transistor and Field Effect Transistors, IEEE Journal of Solid State Circuits, SC-5, June 1970.
89. H. C. Lin, Silicon Contact for Area Reduction of Integrated Circuits, IEEE Transaction on Electron Devices, ED-17, August 1970.
90. E. R. Lippincott, P. R. Griffiths and P. J. Schuhmann, Thermodynamic Equilibria from Plasma Sources, III. Carbon-Hydrogen-Nitrogen Systems, J. Phys. Chem. 74, 2916 (1970).
91. E. R. Lippincott, D. M. Thomas, J. B. Bates and A. Bandy, Single-Crystal Infrared and Raman Spectra of Cyanuric Chloride, J. Chem. Phys. 53, 9 (1970).
92. E. R. Lippincott and G. R. Anderson, Vibronic Effects in Hydrogen Bonding, J. Chem. Phys. 55, 8 (1971).
93. E. R. Lippincott, R. R. Stromberg, W. H. Grant and G. L. Cessac, Polywater - A Search for Alternative Explanations, J. Colloid Interface Science 36, 443 (1971).
94. E. R. Lippincott, R. K. Khanna, G. Cessac and A. R. Bandy, Long Wavelength Phonon Spectra of $\text{Na}_2\text{AlCl}_4 \cdot 3\text{H}_2\text{O}$ and $\text{Na}_2\text{AlCl}_4 \cdot 3\text{H}_2\text{O}$, Spectrochim. Acta., in press.
95. M. J. Marcinkowski and E.S.P. Das, Dislocation Behavior at Grain Boundaries Under Heterogeneous Shear, Journal of Mat. Sci. and Engr. 8, 189 (1971).

96. M. J. Marcinkowski and E.S.P. Das, Propagation of Slip Across a Twist Boundary by Means of Grain Boundary Twist Disclination Loops, Journal of Applied Physics 42, 4107 (1971).
97. M. J. Marcinkowski, J. Czernichow, J. Godes and W. F. Tseng, Twist Boundaries in Ordered Alloys, Metall. Trans. 2, 2185 (1971).
98. M. J. Marcinkowski, Computer Techniques Employed in Lisslocation Analyses, Advances in Materials Research, edited by Herbert Harman 5, 443 (1971), published by Wiley-Interscience, New York.
99. M. J. Marcinkowski and W. F. Tseng, Dislocation Behavior at Tilt Boundaries of Infinite Extent, Metallurgical Transactions 1, 3397 (1970).
100. M. J. Marcinkowski, J. F. Jackson, J. Breedon and M. E. Taylor, Jr., Scanning Electron Microscope Study of Polyethylene Spherulite, J. Polymer Sci., A-2, in press.
101. P. H. Mazzocchi and K. J. Crowley, The Photochemistry of Olefins, The Chemistry of Alkenes, S. Patai Ed., Interscience Publishers, (1970).
102. P. H. Mazzocchi, R. S. Lustig and G. W. Craig, On the Photoisomerizations of 2-methylphenylcyclopropanes. Deuterium Labeling, J. Am. Chem. Soc. 92, 2169 (1970).
103. P. H. Mazzocchi and R. C. Ladenson, The Photoisomerization of 2-Cyclopropyl-1-phenylethylene, Chem. Comm. (1970).
104. P. H. Mazzocchi and H. J. Tamburin, On the Mechanism of the Vinylcyclopropane Cyclopentene Rearrangement. Evidence Against a Concerted Process, J. Amer. Chem. Soc. 92, 7220 (1970).
105. P. H. Mazzocchi, G. R. Miller and H. J. Tamburin, Upfield and Downfield Shifts in the Nuclear Magnetic Resonance Spectrum of a Tris(Dipivalomethanato) Europium(III) Complex, Tetrahedron Letters No. 21, 1819 (1971).
106. G. R. Miller, P. H. Mazzocchi and H. J. Tamburin, Upfield and Downfield Shifts in the Nuclear Magnetic Resonance Spectrum of a Tris(Dipivalomethanato) Europium(III) Complex, Tetrahedron Letters No. 21, 1819 (1971).
107. V. J. Minkiewicz, Critical and Spin-Wave Fluctuations in Ferromagnets by Neutron Scattering, Int'l Journal of Magnetism 1, 165 (1971).
108. V. J. Minkiewicz, K. Gesi and Hirahara, Magnetic Critical Phenomena in MnF by Neutron Scattering, Journal of Applied Phys. 42, 1374 (1971).
109. V. J. Minkiewicz, G. Shirane and A. Linz, Neutron Scattering Study of the Lattice Dynamical Phase Transition in KMnF₃, Solid State Comm. 8, 1941 (1971).
110. V. J. Minkiewicz and D. E. Cox, Magnetic Ordering and Low Ni²⁺ Moment in CsNiCl₃, Phys. Rev. B 4, 2209 (1971).
111. V. J. Minkiewicz, E. B. Osgood, T. A. Kitchen and G. Shirane, Inelastic Neutron Scattering from bcc He, Phys. Rev., to be published.
112. T. C. O'Haver, The Application of Field Effect Transistors as Precision Analog Switches in Laboratory Instrumentation, Chem. Instrumentation 3, 1 (1971).

113. T. C. O'Haver and J. D. Winefordner, Comparison of Analytical Curves in Atomic Fluorescence Spectrometry with Inorganic Fluorometry, Fluorescence News, 5(5), 1 (1971).
114. T. C. O'Haver, Lock-in Amplifiers, J. Chem. Educ., in press.
115. T. C. O'Haver and J. D. Winefordner, Signal-to-Noise Ratio in Atomic Fluorescence Spectrometry and Condensed-Phase Fluorometry, Fluorescence News, in press.
116. T. C. O'Haver, Voltage-to-Frequency Converter, Electronics, in press.
117. T. C. O'Haver, J. D. Winefordner and S. G. Schulman, Luminescence Spectrometry in Analytical Chemistry, Wiley-Interscience, in press.
118. R. E. Prange, Diamagnetic Susceptibility at the Transition to the Superconducting State, Phys. Rev. B 1, 2349 (1970).
119. R. E. Prange and S. P. Singhal, Magnetic Surface Levels in a Tipped Magnetic Field, Phys. Rev. B 2, 4083 (1971).
120. R. E. Prange and V. Korenman, Line Width of Ferromagnetic Resonance in Metals, Journal of Magnetic Resonance, in press.
121. J. V. Sengers, A. M. Wims, D. McIntyre and J. Shereshevsky, Interfacial tension of 3-methylpentane-nitroethane Near the Critical Point, J. Chem. Phys. 52, 3042 (1970).
122. J. V. Sengers and W. R. Hoegy, Three-particle Collisions in a Gas of Hard Spheres, Phys. Rev. A 2, 2461 (1970).
123. J. V. Sengers and P. H. Keyes, Scaling of the Thermal Conductivity Near the Gas-Liquid Critical Point, Phys. Rev. Letters 26, 70 (1971).
124. J. V. Sengers, Triple Collision Effects in the Transport Properties for a Gas of Hard Spheres, in Kinetic Equations, R. L. Liboff and N. Rostoker, Eds. (Gordon and Breach, New York, 1971). pp. 137-193.
125. J. V. Sengers, J. Kestin and E. Paykoc, On the Density Expansion for Viscosity in Gases, Physica 54, 1 (1971).
126. B. F. Smith and C. V. Stevens, Crosslinking Cotton Cellulose with Ethylene Urea Derivatives Having Varying Hydrogen-Bonding Capabilities. Part I: Effects on the Physical Properties and the Hydrogen-Bonded Structure, Textile Research J. 40, 749 (1970).
127. B. F. Smith and C. V. Stevens, Crosslinking Cotton Cellulose with Ethylene Urea Derivatives Having Varying Hydrogen-Bonding Capabilities. Part II: Accessibility Determinations, J. Applied Polymer Science 14, 1691 (1970).
128. B. F. Smith, K. McDonald and R. Dardis, Flammable Fabrics and the Cost of Consumer Protection, Textile Research J. 41, 492 (1971).
129. B. F. Smith, K. McDonald and R. Dardis, An Investigation of Burn Injuries in an Urban Area - 162 Cases, Journal of Fire and Flammability 3, (No. 4), 82 (1971).

130. B. F. Smith, K. McDonald and R. Dardis, Accidental Burn Injuries and Textile Products: A Review, Textile Chemist and Colorist 3 (No. 4), 82 (1971).
131. T. G. Smith and R. Heck, Acetylene Hydrogenation in a Bubble Column Slurry Reactor, I & EC Process Desig. & Dev. 9, 537 (1970).
132. T. G. Smith and K. Wagaman, Use of Hydrocarbons as Carrier Gases in GLC, Journal of Chromatographic Science 9, 241 (1971).
133. T. G. Smith and B. See, Fusion Behavior of Linear Polyethylene in Dodecane-a DTA Study, European Polymer Journal 7, 727 (1971).
134. S. E. Sommer, Characterization of Cathodoluminescence from Carbonate Solid Solutions, Chemical Geology, in press.
135. S. E. Sommer, Cathodoluminescence of Carbonates - Geological Applications, Chemical Geology, in press.
136. S. E. Sommer, Selected Area X-ray Luminescence Spectroscopy with the X-ray Milliprobe, J. Appl. Spectroscopy, Submitted for publication.
137. I. L. Spain and S. Segall, The Equations of State of Solid Helium: A Pressure Scale to 20 k.b. High Pressure Measurements at Low Temperature, Cryogenics, 26 (1971).
138. I. L. Spain, C-axis Conduction in Graphite - Proc. Int. Conf. Semimetals and Narrow Band Gap Semiconductors, Dallas 1970 (to be published in J. Phys. Chem. Solids).
139. I. L. Spain and J. A. Woollam, The Longitudinal C-axis Magnetoresistance of Graphite (ρ_{zz} (H_x)) in High Magnetic Fields, Solid State Comm. 9, (1971).
140. I. L. Spain, An Apparatus for the Measurement of the Galvanomagnetic Properties of Solids in the Temperature Range 2-300°K at Pressures up to 12 k.b., submitted to Cryogenics.
141. J. M. Stewart and H. E. Marr, III, The Crystal Structure of Methylene Blue, Chem. Communications 3, 131 (1971).
142. J. M. Stewart, H. L. Ammon, L. L. Replogle, P. H. Watts and K. Katsumoto, Some Chemistry and Crystallography of Heptafulvenothiopheneazulenodihydrothiophene System, J. Am. Chem. Soc. 93, 2195 (1971).
143. J. M. Stewart and W. H. DeCamp, The Molecular Structure of 1, 1-Dimethyl-3-Phenylpyrazolium-5-Oxide, J. of Heterocyclic Chem. 7, 887 (1970).
144. J. M. Stewart, H. L. Ammon and F. H. Watts, Jr., The Crystal Structure of Thiepin 1,1-Dioxide and the Question of the π -Electron Delocalization in the Molecule, Acta Cryst. B 26, 1679 (1970).
145. W. H. Zoller and W. B. Walters, Studies of Weak β Branching in ^{55}Cr and ^{206}Ti Decay, J. Inorg. Nucl. Chemistry 32, 2456 (1970).

146. W. H. Zoller, J. L. Moyers and R. A. Duce, Gaseous Iodine Measurements and Their Relationship to Particulate Lead in a Polluted Atmosphere, *J. Atmos. Sci.* 28, 95 (1971).
147. W. H. Zoller, P. K. Hopke, ^{131}I L. Fasching, E. S. Macias and W. B. Walters, Half Life Variations of ^{131}I samples, *Phys. Rev. C* 3, 1699 (1971).
148. W. H. Zoller, J. L. Moyers and R. A. Duce, Gaseous and Particulate Bromine in a Polluted Atmosphere, *Environ. Sci. & Tech.* (submitted, 1971).
149. W. H. Zoller, G. E. Gordon, E. S. Gladney and A. G. Jones, Trace Elements in the Urban Atmosphere, Proceedings of the ANS Topcial Meeting on Nuclear Methods in Environmental Research, in press.
- *150. D. D. Davis, W. Braun and A. M. Bass, Reactions of $\text{Cl}({}^2\text{P}_{3/2})$: Absolute Rate Constants for Reaction with H_2 , CH_4 , C_2H_6 , CH_2Cl_2 , C_2Cl_4 and C_6H_{12} , *Intl. J. Chem. Kinetics* Vol. II, 131 (1970).
151. D. D. Davis, R. Huie and J. Herron, Absolute Rate Constants for Reaction of Atomic Oxygen with 1-Butene over the Temperature Range of 239 to 493°K, *J. Phys. Chem.*, in press.
152. D. D. Davis, R. Klemm and M. Pilling, A Flash Photolysis-Resonance Fluorescence Kinetics Study of Ground State Sulfur Atoms: I. Rate Parameters for Reaction of $\text{S}({}^3\text{P})$ with $\text{O}_2({}^3\text{D})$, *Intl. J. Chemical Kinetics*, in press.
153. D. D. Davis, W. Braun and M. Pilling, A Flash Photolysis-Resonance Fluorescence Kinetics Study of Ground State Sulfur Atoms: II. Rate Parameters for Reaction of $\text{S}({}^3\text{P})$ with C_2H_4 , *Intl. J. Chemical Kinetics*, in press.
154. D. D. Davis, R. Huie, J. Herron, W. Braun and M. Kurylo, Absolute Rate Constants for Reaction of Atomic Oxygen with Ethylene over the Temperature Range of 232 to 500°K, *J. Chem. Phys.*, in press.

SECTION VII
OTHER SPONSORS

Air Force Office of Scientific Research
Ames Laboratory
Army Research Office - Durham
Atomic Energy Commission
Arnold Engineering Development Corporation, Tennessee
Computer Science Center (University of Maryland)
CSIR
Cornell University (Agric. Exp. Sta.)
DASA
Deutsche Forschungsgemeinschaft
DoD
Goodyear Tire & Rubber Company
National Aeronautics Space Administration
National Bureau of Standards
National Science Foundation
National Research Council - Canada
Naval Research Laboratory
Office of Naval Research
Petroleum Research Fund
Research Board - University of Maryland
Research Corporation
Walter Reed Army Hospital